Biogeochemical responses to late-winter storms in the Sargasso Sea:

III. Estimates of Export Production using ^{234}Th:^{238}U disequilibria and Sediment Traps.

Kanchan Maiti[1*], Claudia R. Benitez-Nelson[1], Michael W. Lomas[2], and Jeffrey W. Krause[3]

[1]Department of Geological Sciences, University of South Carolina, Columbia, SC 29208 USA

[2]Bermuda Institute of Ocean Sciences, St. George's GE 01, Bermuda

[3]College of Ocean and Atmospheric Science, Oregon State University, Corvallis, OR 97331, USA

*Corresponding Author
Now at: Department of Marine Chemistry and Geochemistry
Woods Hole Oceanographic Institution, Clark 447, MS#25
Woods Hole, MA 02543
Email: kmaiti@whoi.edu
Phone: (508) 289-3916
Fax: (508) 457-2193

Second Revision submitted to Deep Sea Research I

January 2009

Abstract

Direct measurements of new production and carbon export in the subtropical North Atlantic Ocean appear to be too low when compared to geochemical based estimates. It has been hypothesized that episodic inputs of new nutrients into surface water via the passage of mesoscale eddies or winter storms may resolve at least some of this discrepancy. Here, we investigated particulate organic carbon (POC), particulate organic nitrogen (PON), and biogenic silica ($BSiO_2$) export using a combination of water column ^{234}Th:^{238}U disequilibria and free-floating sediment traps during and immediately following two weather systems encountered in February and March 2004. While these storms resulted in a 2-4 fold increase in mixed layer NO_3 inventories, total chlorophyll *a* and an increase in diatom biomass, the systems was dominated by generally low ^{234}Th:^{238}U disequilibria, suggesting limited particle export. Several ^{234}Th models were tested, with only those including non-steady state and vertical upwelling processes able to describe the observed ^{234}Th activities. Although upwelling velocities were not measured directly in this study, the ^{234}Th model suggests reasonable rates of 2.2 to 3.7 m d^{-1}.

Given the uncertainties associated with ^{234}Th derived particle export rates and sediment traps, both were used to provide a range in sinking particle fluxes from the upper ocean during the study. ^{234}Th particle fluxes were determined applying the more commonly used steady state, 1-dimensional model with element/^{234}Th ratios measured in sediment traps. Export fluxes at 200 m ranged from 1.91 ± 0.20 to 4.92 ± 1.22 mmol C m^{-2} d^{-1}, 0.25 ± 0.08 to 0.54 ± 0.09 mmol N m^{-2} d^{-1}, and 0.22 ± 0.04 to 0.50 ± 0.06 mmol Si m^{-2} d^{-1}. POC export efficiencies (Primary Production/Export) were not significantly different from the annual average or from time periods without storms, although absolute POC fluxes were elevated by 1-11%. This increase was not sufficient, however, to resolve the discrepancy between our observations and geochemical based estimates of particle export. Comparison of PON export rates with simultaneous measurements of NO_3^- uptake derived new production rates, suggested that only a fraction, < 35%, of new production was exported as particles to deep waters during these events. Measured $bSiO_2$ export rates were more than a factor of two higher ($p < 0.01$) than the annual average, with storm events contributing as much as 50% of annual $bSiO_2$ export in the Sargasso

Sea. Furthermore it appears that 65 - 95% (average 86 ± 14%) of the total POC export measured in this study was due to diatoms.

Combined these results suggest that winter storms do not significantly increase POC and PON export to depth. Rather, these storms may play a role in the export of $bSiO_2$ to deep waters. Given the slower remineralization rates of $bSiO_2$ relative to POC and PON, this transport may, over time, slowly decrease water column silicate inventories, and further drive the Sargasso Sea towards increasing silica limitation. These storm events may further affect the quality of the POC and PON exported given the large association of this material with diatoms during these periods.

Key Words: Episodic Events, Storms, Particle Export, ^{234}Th:^{238}U disequilibria, biogenic silica, organic carbon

Regional Index Terms: Sargasso Sea, North Atlantic Subtropical Gyre, North Atlantic

1. Introduction

A number of recent biogeochemical studies suggest that episodic phenomena, on the order of days to weeks, have a disproportionately large impact on ocean biogeochemistry (Bidigare et al., 2003; Dickey et al., 2001; Ditullio and Laws, 1991; Karl et al., 2001; McGillicuddy et al., 2007; Pesant et al., 2002). These event scale processes include the passage of eddies, frontal interactions, and severe weather, such as hurricanes (Allen et al., 2005; Benitez-Nelson et al., 2007; Walker et al., 2005). Although it is generally accepted that these short-term weather induced mixing events may contribute to changes in phytoplankton biomass (e.g. Cullen et al., 2002; Dugdale, 1998; Nelson and Brzezinski, 1997; Smayda, 1998), their specific impact on community structure and particulate organic carbon (POC) export to depth remain enigmatic. The transient nature of such storm events simply make them difficult to predict and sample. Moreover, the complex interactions and potential time-lags between physical, chemical and biological factors amplify their intricacy and decrease our ability to quantify the magnitude of the oceanic response.

Within the Sargasso Sea located in the North Atlantic subtropical gyre, the passage of weather fronts results in alternating periods of water column stratification, controlling both light availability and the magnitude of nutrient inputs into the euphotic zone (Steinberg et al., 2001). In the winter, deep convective mixing by weather fronts entrains nutrients and primes the system for an annual phytoplankton bloom that follows seasonal re-stratification of the mixed layer (Michaels et al., 1994; Steinberg et al., 2001). Primary production estimates from the Bermuda Atlantic Time-series (BATS) range from ~26 to 45 mmol C m^{-2} d^{-1} (Lipschultz et al., 2002; Steinberg et al., 2001) and is thought to be mainly limited by nitrogen, although phosphorus limitation may also occur (Ammerman et al., 2003). On average, sediment trap data suggests that 6 - 8% of this organic carbon (1.6 – 3.6 mmol C m^{-2} d^{-1}) is exported below the euphotic zone (Lipschultz et al., 2002; Michaels et al., 1994), but these export rates appear too low when compared to geochemical mass balance estimates of new production derived from net oxygen consumption (6.8 - 11.4 mmol C m^{-2} d^{-1}) (Jenkins, 1988; Jenkins and Goldman, 1985; Michaels et al., 1994), or NO_3^- inputs using the ^3He flux gauge (14.6 ± 4.6 mmol C m^{-2} d^{-1}) (Jenkins and Doney, 2003). It has been suggested that the biological

response to short-term mixing and stratification events associated with the passage of storms is a source of new production that remains largely undocumented by current sampling strategies (Lipschultz et al., 2002; Lomas et al., 2008a). In essence, these organic matter export events are missed by the monthly 3-4 day water column and sediment trap deployments at BATS as they are hypothesized to occur during or immediately following the passage of a frontal system when ship-based measurements are least likely to occur

Here, we investigate the role of storms on POC, particulate organic nitrogen (PON), and biogenic silica ($bSiO_2$) export using ^{234}Th:^{238}U disequilibria and sediment trap measurements made during the passage of two weather systems in the Sargasso Sea in late winter of 2004. Several ^{234}Th export models that include both non-steady state and physical dynamics are tested and used to describe the data. This work was conducted as part of a larger interdisciplinary program to quantify the impact of event-scale processes on Sargasso Sea surface ocean biogeochemistry (Krause et al., 2008; Lomas et al., 2008a; Lomas et al., 2008b). Results are discussed in the context of the physical regime, biological community structure, and other estimates of new production and particle export in the system.

2. Methodology

Samples were collected on board the R/V *Oceanus* from February 15th to March 15th, 2004. A key objective was to avoid sampling eddies, as these physical features are known to increase primary production and potentially enhance particle export and dissolved organic matter accumulation via the upwelling of new nutrients from depth (Benitez-Nelson et al., 2007; McGillicuddy et al., 2007). In order to avoid these mesoscale features, sea level anomaly (SLA) maps were provided by D. McGillicuddy (WHOI) prior to and during the cruise. Once on station, a drogue was deployed at 10 m in the eddy-free areas (SLA ~ 0 cm) in order to minimize sampling of different water masses and maintain a Lagrangian sampling scheme. All the CTD and water sampling were conducted within 0.5 km of the drogue position. This sampling protocol was repeated throughout the cruise. ^{234}Th samples were collected during two drogue deployments (Figure 1). The sampling stations were grouped into two time periods.

Samples along the West Transect (referred to as 2004-1 by Lomas et al., 2008a) were collected from February 18 (Year Day or YD48) to March 1, 2004 (YD61) from 30.5°N to 29°N at 63°W. Samples along the East Transect (referred to as 2004-2 by Lomas et al., 2008a) were collected from March 6 – 14 (YD 66 to YD74), 2004 from ~30.5^{o}N to 30^{o}N at 62.5^{o}W (Figure 1, Lomas et al., 2008a). Profiles of total ^{234}Th were collected from 9 separate casts using a CTD rosette with 12-L Niskin bottles. Each ^{234}Th profile consisted of 12 sampling depths between 0 – 250 m. Deep water samples (3000 m) were also collected from three separate stations in order to confirm beta detector calibration.

In order to quantify gravitational particle flux, a surface-tethered particle interceptor trap (PIT) (Knauer et al., 1979) was deployed for 3–4 day periods at a depth of 200 m. A total of four sediment trap arrays were deployed during the cruise. During each transect two sediment trap arrays were placed in series, such that as soon as one set of traps was recovered the other set was deployed. Deployment, recovery, design and quantification of POC and PON were done as described by Knap et al., (1997). Briefly PIT sample tubes (0.0039 m^2 in surface area) were filled with a formalin (~0.7%) and brine (0.86 mol NaCl L^{-1}) solution. Acid-cleaned (10% HCl) and rinsed 0.8 μm, 76 mm diameter polycarbonate filters were fitted at the base of each sample tube prior to deployment. A drain plug at the bottom of the tube allowed the sample to be drained directly through the filter. After filtration, the filters were placed in acid-cleaned, pre-combusted glass Petri dishes, sealed with parafilm and stored at 4ºC until further processing. PIT tube filtrates (supernatant) was analyzed for silicate using the method outlined by Strickland and Parsons (1972) (see Krause et al., 2008). PIT filters were also analyzed for $bSiO_2$ using a NaOH digestion method (Brzezinski and Nelson, 1995; Paasche, 1973). For POC and PON, swimmers were removed by manual picking. For $bSiO_2$, samples were left intact as significant contamination by swimmers is unlikely in this environment (Brzezinski and Nelson, 1995; Krause et al., 2008).

2.1. CTD and Meteorological Sensor Data.

A suite of meteorological sensors (e.g., temperature, relative humidity, barometric pressure, shortwave radiation, wind speed and direction), mounted on a mast at the ship's bow, collected data throughout the cruise every 10 minutes. These datasets were

averaged hourly and used to calculate the daily net heat flux using the Berliand Approximation in the Air-Sea MATFile routine in MATLAB (The MathWorks Inc., Natick Massachusetts, USA). The calculated net heat flux was used in conjunction with CTD data to identify periods of water column destabilization/stabilization following the passage of storms.

2.2. *^{234}Th Analyses*

All total ^{234}Th water column samples were processed according to the methods described by Pike et al. (2005). Briefly, within 1 h of collection unfiltered 4-liter samples collected for total ^{234}Th determination were acidified to pH ~2. Samples were shaken vigorously and ^{230}Th added as a yield monitor. The samples were shaken again and allowed to equilibrate for >8 hours. Concentrated NH_4OH was subsequently added to each sample to adjust the pH to ~8. Extraction of thorium from seawater was then accomplished by co-precipitation via a MnO_2 precipitate, formed by the addition of both $KMnO_4$ and $MnCl_2$ (Benitez-Nelson et al., 2001a; Benitez-Nelson et al., 2001b; Buesseler et al., 2001; Rutgers van der Loeff et al., 2006). Samples were then shaken vigorously and allowed to stand for 8 hours, prior to filtration onto 25-mm-diameter QMA filters. The filtered Mn precipitates were air dried and mounted on plastic RISO cups under one layer of plastic film and two layers of standard aluminum foil for beta counting (Rutgers van der Loeff et al., 2006). All sediment trap samples collected for POC analysis were directly counted for ^{234}Th activity using the methods described by Buesseler et al. (1995).

All ^{234}Th samples were counted directly on a 5-sample gas-flow proportional low-level RISØ beta counter that measured the beta activity of the highest energy ^{234}Th daughter, ^{234m}Pa (E_{max} = 2.3 MeV). All samples were counted for at least 18 hours or until the counting error was < 3%. Samples were recounted after >150 days (~6 half lives) had passed since collection to precisely determine background count rates, which averaged 0.51 ± 0.05 cpm. Detector calibration was confirmed with > 3000 m deep water samples (assumed to be in radioactive equilibrium), collected from three different casts, five bottles per cast. Replicate deep water samples varied by less than 5%. The average

detector efficiencies for the deep water samples were 0.45 ± 0.02 which is well within the range of our previous estimates.

Once the total ^{234}Th samples were recounted for their background activity, all the filters were removed from the RISØ cups and purified using ion exchange chemistry. Recovery of the added ^{230}Th yield monitor was quantified by inductively coupled plasma-mass spectroscopy with addition of a ^{229}Th internal standard (Pike et al., 2005). Corrections were applied to ^{234}Th activities on the basis of ^{230}Th recoveries. The average recovery was 0.92 ± 0.06. All data are decay corrected to the time of collection and reported with a propagated error that includes uncertainties associated with counting, sample volume, and other measurement errors.

2.3. POC, PON and $bSiO_2$ Analyses

A total of four sets of sediment traps were deployed during the two transects. POC and PON fluxes were measured according to Knap et al., (1997), which includes treatment by HCl acid-fuming for decarbonation prior to analysis. The $bSiO_2$ fluxes were estimated following the methods outlined by Brzezinski and Nelson (1995). All trap samples were also counted for ^{234}Th activity prior to chemical analysis. The samples were then sub-sampled for POC, PON and $bSiO_2$ analysis after final counting for ^{234}Th, thus enabling the particulate ratio of each element to ^{234}Th to be determined.

3. Results and Discussions

3.1. *Brief overview of biology and physics*

The West Transect was dominated by consistently negative net surface heat fluxes with significant heat loss events due to the passage of winter storms near the beginning and end of the sampling period (Figure 2A). Observed mixed layer depths (MLD), based upon a 0.125 kg m^{-3} increase in sigma-t from ~5 m depth (Gardner et al., 1995), remained stable at 120 - 140 m throughout this transect (Figure 2B, Figure 3). However sampling was suspended for 36 hours during YD50-51, and is associated with a factor of two increase in 0-140 m integrated NO_3^-, suggesting rapid mixing followed by restratification. In response to this nutrient injection, total chlorophyll *a* (TChl *a*) concentrations over the

upper 100 m nearly doubled, increasing from ~ 10 to 17 mg m^{-2} (Lomas et al., 2008b), with 100-160 m integrated TChl *a* concentrations increasing by a factor of four, from 2 to 8 mg m^{-2}. This period of continuous convective mixing (relative to the East Transect), had daily 0-140 m integrated $^{15}NO_3^-$ uptake rates of 2.4 ± 1.4 mmol N m^{-2} d^{-1} and daily 0-140 m integrated ^{14}C based primary production rates of 32.5 ± 5.5 mmol C m^{-2} d^{-1} (Lomas et al., 2008a).

In contrast to the West Transect, the East Transect was punctuated by pulsed stratification/destratification events. A net heat gain occurred over the first 3 days (YD66-YD68), mainly associated with a maximum in solar radiation during mid to late afternoon (Figure 2C). The MLD shoaled from 200 to ~125 m (Figure 2D, Figure 3), and was associated with a decline in TChl *a* concentrations that were still significantly higher (≥ 25 mg m^{-2}) than those observed in the West Transect. On YD69-70 there was a storm event, characterized by ~14 m s^{-1} wind speeds that led to a short-lived deepening of the MLD to 170 m, a 3 to 4 fold increase in NO_3^- concentrations at 50 m, and a rapid (1-2 d) doubling of 0-100 m integrated TChl *a* from ~ 25 mg m^{-2} to 45 mg m^{-2} (Lomas et al., 2008b). This TChl *a* increase was coincident with a significant increase in diatom biomass (from < 5% to ~10% of TChl *a*) at the base of the euphotic zone (0-100 m) as confirmed by microscopic and pigment analyses (Lomas et al., 2008b). The short-lived diatom bloom was subsequently followed by a transition in plankton community to haptophytes and then cyanobacteria (Lomas et al., 2008b). This period of pulsed stratification/destratification mixing had daily 0-140 m integrated $^{15}NO_3^-$ uptake rates of 1.7 ± 0.4 mmol N m^{-2} d^{-1} and daily 0-140 m integrated ^{14}C based primary production rates of 62.5 ± 11.6 mmol C m^{-2} d^{-1} (Lomas et al., 2008a).

3.2. *^{234}Th flux estimates*

3.2.1. *Steady state ^{234}Th fluxes*

Total ^{234}Th activities varied both with depth and station location, ranging from 2.16 to 2.76 dpm L^{-1}. In general, largest ^{234}Th:^{238}U disequilibria occurred in the upper 150 m of each transect, suggesting that this depth region is where rates of particle formation and sinking are highest (Figure 4). Activities greater than secular equilibrium were typically found between 150 - 250 m and attributed to particle remineralization.

The export flux of ^{234}Th at a particular depth can be estimated by solving the following activity balance equation for total ^{234}Th in the ocean (Buesseler et al., 1992; Cochran et al., 1995; Savoye et al., 2006).

$$\partial A_{Th}/\partial t = \lambda_{Th}(A_U - A_{Th}) - P_{Th} + V \quad (1)$$

where $\partial A_{Th}/\partial t$ is the change in total ^{234}Th activity with time, A_U is the ^{238}U activity determined from salinity ($^{238}U = 0.0686 \times$ salinity $\times$ density; Chen, 1986), A_{Th} is the measured activity of total ^{234}Th, λ_{Th} is the decay constant for ^{234}Th (= 0.0288 d^{-1}), P_{Th} is the net removal flux of ^{234}Th on particles, and V represents the sum of advective and diffusive processes (Buesseler et al., 1992; Savoye et al., 2006). In most studies, steady state (SS) is assumed ($\partial A_{Th}/\partial t = 0$) and physical processes are considered negligible (V = 0) (e.g. Savoye et al., 2006), reducing equation (1) to:

$$P_{Th} = \lambda_{Th}(A_U - A_{Th}) \quad (2)$$

Solving this equation and integrating over the depth of interest provides a measure of the total flux of ^{234}Th removed from a specific depth horizon via sinking particles, i.e.

$$P_{Th} = \lambda_{Th} \int [A_U - A_{Th}]dz \quad (3)$$

Using the total ^{234}Th measured in the upper 200 m of the water column, the SS particle flux (P_{Th}) of ^{234}Th was first determined using Equation 3. In the West Transect, SS ^{234}Th fluxes varied from to 484 ± 197 to 1071 ± 175 dpm m^{-2} d^{-1} (Table 1, Figure 5), with an average of 896 ± 248 dpm m^{-2} d^{-1} (n = 5). In the East Transect, SS ^{234}Th fluxes were much lower, 283 ± 197 to 808 ± 205 dpm m^{-2} d^{-1}, with an average of 505 ± 252 dpm $m^{-2}d^{-1}$ (n = 3). These SS export fluxes are similar to those measured previously in the North Atlantic Subtropical Gyre (e.g. Thomalla et al., 2006). Two sediment trap deployments were conducted within each transect. The particles collected in the sediment trap samples provide average (± std. dev.) sediment trap based ^{234}Th flux estimates of 617

± 219 dpm m^{-2} d^{-1} and 957 ± 274 dpm m^{-2} d^{-1} for the West and East Transects, respectively.

3.2.2 *Non-steady state ^{234}Th fluxes*

In most ^{234}Th export applications, limited field sampling necessitates that only a SS model ^{234}Th flux model can be used, i.e. assuming no change in ^{234}Th activity with time ($\partial A_{Th}/\partial t$, = 0 in Equation 1). However, rapid temporal changes in upper water column ^{234}Th activity have been documented following large phytoplankton blooms (Buesseler et al., 2005; Buesseler et al., 1992; Cochran et al., 1997; Tsunogai et al., 1986; Wei and Murray, 1992), thereby substantially affecting ^{234}Th derived particle export rates. For example, if the non-steady term (NSS) is positive, due to an increase in water column ^{234}Th activities with time ($\partial A_{Th}/\partial t > 0$), than ^{234}Th derived particle export rates (P_{Th} in equation 1) would decrease. In essence, not including the NSS term, $\partial A_{Th}/\partial t$, would result in an *over*estimation of the ^{234}Th flux. The opposite would occur if the NSS term was negative.

In this study, both of the sampling transects show large changes in TChl *a* over the course of sampling and a statistically significant and progressive decrease in the SS ^{234}Th flux with time (West $r^2 = 0.97$, $p < 0.01$; East $r^2 = 0.93$, $p < 0.05$). In other words, water column ^{234}Th activities increased with time back into secular equilibrium with ^{238}U. This suggests that sampling along both transects may have occurred after an export event (e.g. the demise of a small phytoplankton bloom) that scavenged ^{234}Th from the system, with a greater export event associated with the East versus the West Transect. It is possible that some of this variability may be due to submesoscale patchiness within a single water mass or sampling of different water masses as the ship followed the drifter. However, analysis of temperature-salinity diagrams show no evidence of non-Lagrangian sampling and the significance in SS flux trends suggests a coherent rather than random temporal trend. Given the high resolution sampling that occurred on each transect, we therefore have a rare opportunity to investigate NSS processes and its influence on ^{234}Th flux models (e.g. Savoye et al., 2006).

In order to assess NSS influences, we calculated depth-weighted average ^{234}Th activities (dpm L^{-1}) over time for four different depth intervals, 0-50 m, 0-100 m, 0-150

m and 0-200 m, following the procedure in Buesseler et al. (1992, Appendix A). The temporal change in ^{234}Th activity was then plotted for each transect and fitted using a linear regression (Figures 6 and 7, Table 2). The largest variability for both transects was observed in the upper 50 m (Figures 6 and 7), likely due to patchiness in biological activity (Figure 3; Lomas et al., 2008b). Most of the depth integrated data fall within the 95% confidence limits of the linear fit (Figures 6 and 7) with calculated standard errors on the slopes ranging from 13% for the 0–200 m depth integral to 65% for the 0–50 m layer (Table 2). Using the calculated slope and error (Table 2), we determined a NSS term ($\partial A_{Th}/\partial t$) for the upper 0-200 m of -2600 ± 338 and -3400 ± 468 dpm m^{-2} d^{-1} for West and East Transects. Assuming physical processes to be negligible these *negative* NSS terms resulted in 200 m ^{234}Th fluxes in the range of -1529 ± 380 to -3318 ± 508 dpm m^{-2} d^{-1} for the West and East Transects (Figure 5, Table 1).

Negative ^{234}Th fluxes have no physical meaning and we reiterate that natural spatial variability in biological activity cannot be discounted, nor can one ensure that the same water mass is repeatedly sampled down to depths of 200 m. Nonetheless, these quite large negative fluxes suggest that other sources of ^{234}Th activity, such as physical processes, have not been sufficiently incorporated into the ^{234}Th model and must be considered.

3.2.3. *Effects of physical processes on ^{234}Th fluxes*

The influence of physical mixing processes on the ^{234}Th flux model may be substantial, especially when ^{234}Th fluxes are low (500 – 1000 dpm m^{-2} d^{-1}, Savoye et al., 2006) or in regions of strong upwelling, which injects ^{234}Th-rich deep waters back into the surface ocean (Buesseler et al., 1995; Dunne and Murray, 1999). Rapid changes in NO_3^- inventories, variability in MLD and isopycnal surfaces (Figure 3), and large negative ^{234}Th NSS fluxes all strongly suggest that physical processes played an important role in the spatial and temporal distribution of ^{234}Th activity in the upper 200 m. We tested this hypothesis using a simple box model formulation.

The average depth-weighted, 0-200 m ^{234}Th activity of the first station sampled in each transect is used as the initial ^{234}Th activity of the water mass in the time-series. In this box model, any subsequent loss of ^{234}Th is either due to radioactive decay or

downward vertical flux on sinking particles. Any subsequent addition of ^{234}Th is either due to ingrowth from ^{238}U or from an external source, e.g. physical processes. Assuming that the water mass from the first station of each transect behaved as a isolated body (due to Lagrangian sampling), we applied a ^{234}Th decay and ingrowth correction and calculated the expected ^{234}Th activity for all of the other stations along each transect assuming no ^{234}Th is removed ($P_{Th} = 0$ in Equation 1) (Faure and Mensing, 2005):

$$A_{Th}^{n} = \frac{\lambda_{Th} A_U (e^{-\lambda U (t_n - t_1)} - e^{-\lambda Th (t_n - t_1)})}{\lambda_{Th} - \lambda_U} + A_{Th}^{1} e^{-\lambda Th (t_n - t_1)} \qquad (4)$$

where A_{Th}^{n} is the total activity of ^{234}Th for station n, A_U is the activity of ^{238}U derived from salinity (Chen, 1986), A_{Th}^{1} is the average 0-200 m activity of ^{234}Th in the first station in the time series, t_1 is the date of sampling for the first station, t_n is the date of sampling for station n, λ_{Th} is the decay constant of ^{234}Th and λ_U is the decay constant of ^{238}U. Note that this equation is similar to that used in Savoye et al. (2006), but does not assume that λ_U is negligible. This exercise demonstrates that ingrowth and decay alone do not account for the rapid increase in ^{234}Th activity observed with time (Figure 8, open squares).

Incorporating a removal flux of ^{234}Th on sinking particles results in the following equation:

$$A_{Th}^{n} = \frac{\lambda_{Th} A_U (e^{-\lambda U (t_n - t_1)} - e^{-\lambda Th (t_n - t_1)})}{\lambda_{Th} - \lambda_U} + A_{Th}^{1} e^{-\lambda Th (t_n - t_1)} - P_{Th}(t_n - t_1) \qquad (5)$$

where P_{Th} is the particle flux of ^{234}Th at 200 m using the 200 m sediment trap results (West: 617 ± 219 and East: 957 ± 274 dpm m^{-2} d^{-1}) translated into dpm L^{-1} d^{-1} (East: 0.003 ± 0.001 and West: 0.005 ± 0.001 dpm L^{-1} d^{-1}).

As expected, adding a ^{234}Th flux term decreases the calculated ^{234}Th activities below that determined from ingrowth and decay (Figure 8, open diamonds) and is hence even lower than that directly observed (Figure 8, closed circles). This again indicates that

an additional source of ^{234}Th-rich water into the system, e.g. by physical processes, is needed for mass balance.

Physical inputs of ^{234}Th into our simple box model can be both diffusive and advective. Horizontal diffusive fluxes are likely to be quite small in the Sargasso Sea. An earlier study at the BATS site (Buesseler et al., 1994) determined a horizontal dimensionless Peclet number (P_e), which scales the importance of advection versus eddy diffusion, of 2 x 10^4. This clearly demonstrated that advective horizontal fluxes dominate in the region. In order for the vertical diffusive fluxes to play an important role in the ^{234}Th mass balance, an excess ^{234}Th inventory (^{234}Th activity > ^{238}U activity) below 200 m must be large enough to balance the observed ^{234}Th sediment trap fluxes. A typical open ocean (Sargasso Sea) vertical eddy diffusivity of 0.1 x 10^{-4} m^2 s^{-1} (Buesseler et al., 1994) requires a gradient in ^{234}Th activity that is at least 0.70 dpm L^{-1} m^{-1}. This would mean an excess ^{234}Th activity greater than 1.0 dpm L^{-1} just a few meters below the 200 m sediment trap. ^{234}Th excess activities observed during this study were in the range of 0.01 - 0.09 dpm L^{-1} at a depth of 250 m, an order of magnitude too low (Figure 4). We have therefore restricted the following formulation to a simple box model that incorporates the physical addition of higher activity ^{234}Th water from an external source by advection only. In this study, sampling was conducted in a Lagrangian fashion. We therefore consider horizontal advection to be minimal. Rapid changes in NO_3^- inventories as well as variability in MLD and isopycnal surfaces along both transects (Figure 3) strongly suggests that upwelling is the source of the ^{234}Th entering the system.

Equation 5 is thus further modified to include an upwelling input term of relatively ^{234}Th rich water from below:

$$A_{Th}^{n} = \frac{\lambda_{Th} A_U (e^{-\lambda_U (t_n - t_1)} - e^{-\lambda_{Th} (t_n - t_1 1)})}{\lambda_{Th} - \lambda_U} + A_{Th}^{1} e^{-\lambda_{Th} (t_n - t_1)} - P_{Th}(t_n - t_1) + I_{Th}(t_n - t_1) \quad (6)$$

where I_{Th} is the constant rate (in dpm L^{-1} d^{-1}) at which ^{234}Th enters the system by upwelling. We calculated a best fit for I_{Th} between the observed and modeled West

Transect data of 0.0066 dpm L^{-1} d^{-1} (χ^2 = 0.00029). In the East Transect, I_{Th} was calculated to be 0.0114 dpm L^{-1} d^{-1} (χ^2 = 0.00028) (Figure 8, open triangles).

While the addition of an upwelling term now describes the temporal evolution of observed 0-200 m integrated ^{234}Th activity (Figure 8), it does not provide any information on the upwelling rate. In order to examine if upwelling rates are reasonable, we defined the vertical upwelling component as follows:

$$V = w\frac{\partial A_{Th}}{\partial z} \qquad (7)$$

where w is the upwelling velocity and $\partial A_{Th}/\partial z$ is vertical gradient in ^{234}Th activity. The vertical ^{234}Th gradient, $\partial A_{Th}/\partial z$, was estimated from the ^{234}Th activity between 200 and 250 m. The average ^{234}Th activities at 200 m are 2.387 ± 0.08 and 2.390 ± 0.08 dpm L^{-1} for the West and East transects respectively, while the average ^{234}Th activities at 250 m are 2.538 ± 0.10 and 2.542 ± 0.10 dpm L^{-1}. From this data we estimated an average ^{234}Th vertical-gradient to be 0.0030 ± 0.0002 dpm L^{-1} m^{-1} for both Transects. From Equation 6, we have already estimated that an input term (I_{Th}) of 0.0066 and 0.0114 dpm L^{-1} d^{-1} for the West and East Transects are needed to balance the system. Hence, if upwelling is the sole source of this input, we can equate V and I_{Th}, which translates to:

$$I_{Th} = w\frac{\partial A_{Th}}{\partial z} \qquad (8)$$

Solving for w results in an estimated storm induced upwelling rates of 2.2 and 3.7 m d^{-1} for the West and East Transects, respectively. Note that increasing the particle flux term derived from the sediment traps (P_{Th}) increases the upwelling rate, and vice versa. Assuming an uncertainty of ± 50% associated with the sediment traps results in an upwelling rate uncertainty of ± 0.5 and ± 0.8 m d^{-1} for the West and East Transects, respectively. These upwelling rates seem reasonable, especially upon closer examination of the depth versus density profiles (Figure 3), where the isopycnal surfaces in the East Transect are more strongly uplifted than those in the West transect. For comparison, a modeling and tracer release experiment within several Sargasso Sea mesoscale eddies by McGillicuddy et al. (2008) suggested upwelling velocities of 0.4 – 1.6 m d^{-1}.

3.2.4. *^{234}Th flux model summary*

The simple box models used to describe the water column ^{234}Th distributions observed during this study demonstrate that the assumption of SS is likely invalid for this study. Furthermore, coherent temporal changes in ^{234}Th activities suggest that the NSS ^{234}Th model must also include physical processes, e.g. upwelling. These results highlight the importance of often neglected physically processes on ^{234}Th based flux estimates, especially in areas of low ^{234}Th:^{238}U disequilibria. While the assumptions used in the box model (accurate sediment trap fluxes, minimal patchiness) are subject to large errors, the estimated upwelling velocities are consistent and reasonable for the storm induced rapid changes in MLD observed in the West and East Transects. Nonetheless, it is impossible to gauge ^{234}Th export fluxes without bias since advection velocities were not directly measured during the cruise and there is the possibility that an export event may have occurred prior to sampling. Note that these two processes work in opposition with regard to the ^{234}Th mass balance flux model. An export event that precedes sampling will result in an overestimate of the ^{234}Th particle flux, whereas upwelling of ^{234}Th rich water will result in an underestimate of the ^{234}Th particle flux. While it is tempting to ignore any subsequent mention of particle flux using the ^{234}Th water column data, we argue that the traditional application of the SS one-dimensional model should still be discussed and presented for comparison with previous work and simultaneously deployed sediment traps that have their own inherent biases (e.g. Buesseler et al., 2007a). We therefore include the 1-dimensional SS ^{234}Th based POC, PON, and $bSiO_2$ fluxes along with the sediment trap results to provide a range in export estimates.

3.3. *Elemental/^{234}Th ratios*

Translation of water column derived ^{234}Th fluxes into export fluxes of POC, PON, $bSiO_2$ or any other constituent, requires the use of an empirical relationship between a given constituent, X, and particulate ^{234}Th:

$$(P_X)_z = (P_{Th})_z \times (X/^{234}Th)_z \qquad (9)$$

Where $(P_{Th})_z$ is the depth integrated ^{234}Th flux at the lower depth boundary, *"z"*, and $(X/^{234}Th)_z$ is the $X/^{234}$Th ratio measured in sinking particles collected at depth *"z"*. $(P_X)_z$ is thus the sinking particle flux of a given element, X. The key is to measure the $X/^{234}$Th at the base of the depth interval of interest and to use it with the integrated ^{234}Th disequilibrium flux determined over the same depth interval (Benitez-Nelson and Charette, 2004; Savoye et al., 2006). In this study all export fluxes are calculated for a depth of 200 m to compare with the sediment traps.

There are a number of additional methods with which to collect elemental/^{234}Th ratios, such as sediment traps, *in situ* pumps and bottles. In a recent compilation by Buesseler et al. (2006), *in situ* pumps and sediment trap C/^{234}Th ratios generally agreed within a factor of two and this has been confirmed by a number of other studies investigating episodic phenomena in oligotrophic waters (Benitez-Nelson et al., 2007; Benitez-Nelson et al., 2001a; Buesseler et al., 2008; Maiti et al., 2008).

In this study, the ratios of specific constituents (e.g. POC) to ^{234}Th were measured in sediment traps deployed at 200 m. POC/^{234}Th ratios ranged from 3.7 – 6.7 μmol C dpm^{-1}, similar to the 4.9 ± 1.5 μmol C dpm^{-1} previously measured at the BATS site using sediment traps (Buesseler et al., 2006) and the 6.0 – 14.8 μmol C dpm^{-1} measured on a central transect through the North and South Atlantic using *in situ* pumps (Table 3 in Thomalla et al., 2006). Average sediment trap POC/^{234}Th values measured in this study are also well within the ranges found during the diatom blooms in the North Atlantic Bloom Experiment (6 - 10 μmol C dpm^{-1}) and mesoscale eddy programs, E-FLUX (1.5-3.0 μmol C dpm^{-1}) and EDDIES (1.5 - 4.5 μmol C dpm^{-1}) (Buesseler et al., 1995; Maiti, 2007; Maiti et al., 2008; Buesseler et al., 2008;). It is interesting to note that the average sediment trap POC/^{234}Th ratio measured during the West Transect, 4.3 ± 0.8 μmol C dpm^{-1}, is significantly lower ($p < 0.05$) than that measured during the East Transect, 6.6 ± 0.1 μmol C dpm^{-1}. PON/^{234}Th ratios in the sediment traps varied from 0.48 ± 0.05 to 0.87 ± 0.09 μmol N dpm^{-1}, whereas $bSiO_2$/^{234}Th ratios varied between 0.27 ± 0.03 and 0.72 ± 0.06 μmol Si dpm^{-1}. This is again similar to previous investigations like those from the lee of the Hawaiian Islands, where the PON/^{234}Th and $bSiO_2$/^{234}Th ratio in traps varied from 0.14 – 0.28 μmol N dpm^{-1} and 0.20 – 0.40 μmol Si dpm^{-1} (Maiti et al., 2008), and the Sargasso Sea, where PON/^{234}Th ratios of 0.25-0.52 μmol N dpm^{-1} were measured in

traps and a $bSiO_2/^{234}Th$ ratio of 0.11-0.21 measured using *in situ* pumps (trap $bSiO_2/^{234}Th$ ratio not reported, Buesseler et al., 2008).

The 50% higher $POC/^{234}Th$ ratios in the East Transect relative to the West Transect, is likely due to the diatom bloom that occurred during East Transect sampling. We can examine this change more closely using simple surface area to volume arguments. A change in the $POC/^{234}Th$ ratio of a source particle can be assumed to be controlled largely by particle size (Buesseler et al., 2006; Burd et al., 2000). In other words, the ^{234}Th activity on a source particle increases with increasing surface area, while the carbon content should increase as function of particle size (volume). Following this logic, a smaller particle will have higher surface area to volume ratio (SA:V), i.e. lower $POC/^{234}Th$, while larger particles will have lower SA:V ratios, i.e. higher $POC/^{234}Th$. Consistent with this construct is a significant shift in the integrated abundances of pico- and nano-plankton during each Transect (Table 3) (Lomas et al., 2008b). The 'community average' SA/V ratio over the upper 100 m was then determined using the average size and abundance distribution (%) of each class and assuming spherical shapes for all cells. The resulting community average SA/V ratio decreased from 8.2 in the West Transect to 6.2 in the East Transect; a 25% decrease that is consistent with the 54% increase in the $POC/^{234}Th$ ratio observed between the two transects.

It is important to note here that there is a possibility that the element/^{234}Th ratio may be altered to some extent due to selective dissolution within the sediment traps. However, the loss or dissolution of POC and PON to trap supernatants are considered small for the short term (2 - 4 days) shallow trap deployments used in this study. (Buesseler et al., 2007a; Lamborg et al., 2008). Dissolution rates of $bSiO_2$ measured directly in the trap cups were found to be less than < 15% of the total $bSiO_2$ flux (Krause et al., 2008).

3.4. *POC, PON and $bSiO_2$ Export Fluxes*

Elemental fluxes were estimated using two different approaches: direct quantification from the surface tethered PIT style sediment traps and ^{234}Th fluxes derived using a SS one-dimensional model and converted into elemental fluxes using $POC/^{234}Th$, $PON/^{234}Th$ and $bSiO_2/^{234}Th$ ratios of trap materials. In order to compare the observed

sediment trap POC fluxes with ^{234}Th derived POC (PON and $bSiO_2$) fluxes, SS ^{234}Th fluxes and average POC (PON and $bSiO_2$)/^{234}Th ratios from individual stations were averaged over the same time period as that of each sediment trap deployment.

3.4.1. *POC Export*

The sediment trap and ^{234}Th results provide an opportunity to test how particle flux varies under two different physical regimes relative to ambient, non-storm impacted winter conditions, with the West Transect having relatively continuous convective mixing and the East Transect experiencing a pulsed convective mixing event. Both systems were characterized by rapid increases in TChl *a*, and, at least in the East Transect, a doubling in diatom biomass (Lomas et al., 2008a; Lomas et al., 2008b). In this study, average ^{14}C based PP for the upper 200 m was 32.5 ± 5.5 mmol C m^{-2} d^{-1} for the West Transect and 62.5 ± 11.6 mmol C m^{-2} d^{-1} for the East Transect (Lomas et al., 2008a). POC export fluxes at 200 m were ranged from 1.91 ± 0.20 mmol C m^{-2} d^{-1} (Trap based) and 3.90 ± 0.32 mmol C m^{-2} d^{-1} (^{234}Th based) for the West and 4.92 ± 1.22 mmol C m^{-2} d^{-1} (Trap based) and 2.85 ± 1.34 mmol C m^{-2} d^{-1} (^{234}Th based) for the East (Table 4). The average sediment trap POC flux for the East Transect was a factor of ~2 higher than the West Transect ($p < 0.0001$), whereas the ^{234}Th derived POC fluxes showed no statistical difference.

To compare these results with typical winter conditions in the Sargasso Sea, average non-storm impacted winter (December to March) primary production (PP) estimates at the BATS time series station were calculated over a 12-year time period (1990-2002) using only those sample periods with no detectable NO_3 (< 10 nM) in the upper water column (n = 20 sample periods out of 43). The average rate of winter PP was 39.4 ± 4.8 mmol C m^{-2} d^{-1}, with average winter POC fluxes at 200 m of 1.55 ± 1.09 mmol C m^{-2} d^{-1}. While average annual PP estimates are similar, 34.79 ± 5.48 mmol C m^{-2} d^{-1}, average annual POC export rate are more than 50% higher than the winter mean, 2.38 ± 0.33 mmol C m^{-2} d^{-1} (Steinberg et al., 2001).

The carbon export ratios (average of ^{234}Th and sediment trap POC export/PP) for the West and East Transect were 0.09 ± 0.03 and 0.06 ± 0.02, not significantly different from the non- storm impacted winter time ambient conditions of 0.04 ± 0.03, or the

annual average export efficiency of 0.07 ± 0.02. These results suggest that the winter mixing events observed during this study are not more efficient in the transport of POC to deeper waters, despite elevated POC fluxes and the increase in diatom abundance, presumably major contributors to particle flux (Michaels and Silver, 1988). The lack of an increase in export efficiency is similar to that observed for other transient mixing events, such as mesoscale eddies in the North Pacific Subtropical Gyre (Benitez-Nelson et al., 2007; Maiti, 2007), suggesting that rapid remineralization by grazers and conversion of POC to dissolved organic matter plays an important role in determining POC to depth transport efficiencies (Benitez-Nelson et al., 2007). Therefore, in addition to total phytoplankton biomass, knowledge of biological community structure is essential for understanding the mechanisms controlling particle export in the Sargasso Sea.

While the transport efficiency of storm induced events is not significantly different from ambient conditions, they may still play an important role in enhancing overall POC export rates to depth. Using air temperature and wind speed data collected at the Bermuda Testbed Mooring located ~200 km away from the cruise track, approximately 8-10 storm events occur annually (Lomas et al., 2008a). Assuming 10 storm events each lasting 3 days and with a POC export rates ranging from 1.9 mmol C m^{-2} d^{-1} to 4.9 mmol C m^{-2} d^{-1} (minimum and maximum POC flux observed during this study, Table 4), results in a winter storm induced increase of 11-100 mmol C m^{-2} y^{-1}. This results in a 1-11% higher estimate than the average annual POC flux of 869 ± 120 mmol C m^{-2} y^{-1} in the Sargasso Sea. This increase is too low to resolve the current discrepancy in the geochemical based estimates of POC export in the Sargasso Sea (e.g. Jenkins and Doney, 2003).

3.4.2. *PON Export*

Average PON fluxes were 0.25 ± 0.08 (sediment trap) and 0.50 ± 0.17 mmol N m^{-2} d^{-1} (^{234}Th based) for the West Transect and 0.54 ± 0.09 (sediment trap) and 0.30 ± 0.08 mmol N m^{-2} d^{-1} (^{234}Th based) for the East Transect (Table 4, Figure 9). For comparison, average non-storm impacted winter PON fluxes at 200 m are 0.22 ± 0.17 mmol N m^{-2} d^{-1}, the same as the annual average of 0.23 ± 0.17 mmol N m^{-2} d^{-1}. During this study, Lomas *et al* (2008a) used measurements of NO_3^- uptake as a proxy for 'new' nitrogen and

estimated an average new production rate of 2.4 ± 1.4 and 1.7 ± 0.4 mmol N m^{-2} d^{-1} for the West and East Transects, an order of magnitude higher than the observed PON export. In contrast, NO_3^- drawdown rates were significantly lower, 0.38 and 1.1 mmol m^{-2} d^{-1} (Lomas et al., 2008a). The nitrogen export ratios (calculated as average of ^{234}Th and sediment trap PON export/$^{15}NO_3^-$ uptake rates) for the West and East Transects were estimated to be 0.16 ± 0.07 and 0.25 ± 0.10. We consider these values to be overestimates, as other N sources, such as NH_4^+, were not included in the N uptake rates. While our estimated export ratios are significantly higher than the canonical f-ratio of 0.06 for oligotrophic gyres (Eppley and Peterson 1979), they are within the annual range of values (0.08-0.39) reported for the region by Lipschultz (2001). Regardless, these results suggest that only a fraction of the new production generated by the observed storms results in PON export. These results are similar to another separate study by Painter et al. (2007) in the eastern tropical and subtropical North Atlantic, who found that only ~1% of the $^{15}NO_3^-$ uptake they measured at the base of the euphotic zone was associated with NO_3^- drawdown, which they assumed was equivalent to the PON export. It is interesting to note that in this study, only 25-50% (depending on depth) of the NO_3^- drawdown could be attributed to the accumulation of suspended PON and dissolved organic nitrogen (Lomas et al., 2008a). The location of the missing "N" remains unknown, but time scales of the various measurements and the natural variability associated with sub-mesoscale patchiness cannot be discounted in these simple mass balance estimates.

3.4.3. *$bSiO_2$ Export*

Average $bSiO_2$ fluxes were 0.23 ± 0.03 (sediment trap) and 0.29 ± 0.05 mmol Si m^{-2} d^{-1} (^{234}Th based) for the West Transect and 0.50 ± 0.06 (sediment trap) and 0.22 ± 0.04 mmol Si m^{-2} d^{-1} (^{234}Th based) for the East Transect (Table 4, Figure 9). These estimates are significantly higher ($p < 0.01$) than the annual estimated flux of 0.07 – 0.14 mmol Si m^{-2} d^{-1} at 200 m for the Sargasso Sea (Nelson and Brzezinski, 1997).

Krause et al. (2008) measured $bSiO_2$ silica production rates during this study using the ^{32}Si tracer and incubation method described by Brzezinski and Phillips (1997) and Brzezinski et al. (2001). Depth integrated (0 – 140 m) $bSiO_2$ production rates

averaged 1.03 ± 0.96 (n = 17) and 2.28 ± 2.06 (n = 9) mmol Si m^{-2} d^{-1} for the West and East Transects, respectively, a substantial increase over previous Sargasso Sea measurements (Brzezinski and Kosman, 1996; Brzezinski and Nelson, 1995; Nelson and Brzezinski, 1997). For example, Nelson and Brzezinski (1997) reported $bSiO_2$ production rates of only 0.10 to 0.93 mmol Si m^{-2} d^{-1} (mean 0.42 ± 0.22 mmol Si m^{-2} d^{-1}) in a three year study (1992-1994) at BATS. During our cruise, integrated $bSiO_2$ stocks were also enhanced by a factor of 2.5 in the East relative to the West Transects coincident with a temporal increase in vertically integrated $bSiO_2$ (2.5 mmol m^{-2} on YD68 to ~4.5 mmol m^{-2} on YD70) and NO_3^- concentrations (from ~18 mmol m^{-2} to ~55 mmol m^{-2}) (Krause et al., 2008; Lomas et al., 2008a).

Elevated standing stocks and production rates of $bSiO_2$ were also reflected in the higher $bSiO_2$ fluxes recorded in the sediment trap deployed from YD70 to YD74. This enhanced $bSiO_2$ flux was not evident in the ^{234}Th-based $bSiO_2$ fluxes, as only one ^{234}Th derived flux measurement was conducted on YD70. Since $bSiO_2$ data suggest that the bloom started to decline rapidly after YD70, it is likely that most of the $bSiO_2$ flux was missed by this single YD70 ^{234}Th profile. However, this sampling period was also characterized by a ~50% increase in POC/^{234}Th ratio discussed earlier (See Section 3.2). We hypothesize that this increase was caused by the collection of diatom frustules in the sediment trap, as diatoms have a higher surface area to volume ratio due to their 'pill box' shape (Buesseler et al., 1998). This hypothesis also explains the increase in the Si/^{234}Th ratio along the East Transect.

Using the range in Si production and export discussed above, we estimated a Si export efficiency of 0.11 - 0.28 during this study. The average annual estimate of Si production in the Sargasso Sea is 239 mmol Si m^{-2} y^{-1}, i.e. 0.65 mmol Si m^{-2} d^{-1} (Nelson and Brzezinski, 1997), while the average annual Si export is in the range of 0.07 – 0.14 mmol Si m^{-2} d^{-1}. This leads to a mean annual Si export efficiency of 0.11 to 0.21, although not significantly different from that determined in the storm events observed here, this annual export efficiency does not enable specific differentiation from non-storm events.

Krause et al. (2008) estimated an annual $bSiO_2$ export flux of 23 mmol Si m^{-2} y^{-1} using fluxes derived from thermally stratified periods (Nelson and Brzezinski, 1997).

Using our estimate of 10 storm events per year each lasting 3 days, and a range in $bSiO_2$ export rates from 0.22 ± 0.02 to 0.50 ± 0.01 mmol Si m^{-2} d^{-1} (from Table 4), we obtain a winter storm induced increase of 4.5 to 12.9 mmol Si m^{-2} y^{-1}, or 20-50% of the annual $bSiO_2$ export. Thus, episodic nutrient injection events induced by storms may play a significant role in the export of $bSiO_2$ depth. This is similar to recent studies of mesoscale eddies in the Sargasso Sea and the North Pacific (Benitez-Nelson et al., 2007; Buesseler et al., 2008; Maiti et al., 2008). Given the slower remineralization rates of $bSiO_2$ relative to POC and PON, this transport may, over time, slowly decrease water column silicate inventories, and further drive the Sargasso Sea towards increasing silica limitation.

Given the hypothesis that diatoms may disproportionately contribute to the flux of POC to depth (Michaels and Silver, 1988), we estimated the contribution of diatoms to the observed POC flux using a Si/C mole ratio of 0.13 (Brzezinski, 1985; Nelson and Brzezinski, 1997) and assuming that all of the $bSiO_2$ measured in the particles is diatom derived. The Si/C ratio may vary widely as a function of species, depth and silica limitation (Brzezinski, 1992; Martin-Jezequel et al., 2000; Paasche, 1973; Ragueneau et al., 2000). The Si/C ratio of 0.13 used in this calculation is the average ratio derived from culture studies of a wide range of diatom species found in temperate and subtropical regions and grown under nutrient replete conditions (Brzezinski, 1985; Nelson and Brzezinski, 1997). Previous studies at BATS (Brzezinski and Nelson, 1995) suggest that diatom growth is silica limited indicating that the Si/C ratio should be < 0.13 (Brzezinski, 1992; Paasche, 1973) This suggests that a Si/C ratio of 0.13 applied to silica production results in a minimum estimate of POC production by diatoms.

Using these assumptions, we determined that 65 - 95% (average 86 ± 14%) of the total POC export measured in this study was due to diatoms. Dividing mean depth integrated (0-140 m) $bSiO_2$ production rates (West Transect: 1.03 mmol Si m^{-2} d^{-1} and East Transect: 2.28 mmol Si m^{-2} d^{-1} (Krause et al., 2008) by a Si/C ratio of 0.13 results in a POC production estimate of 7.9 and 17.5 mmol C m^{-2} d^{-1} for the West and East Transects, respectively. This suggests that diatoms contribute 24 - 28% of the ^{14}C based PP. Thus diatoms, which are responsible for less than 30% of the PP, contribute more than 50% of the total POC export observed during these two storm events. This further

suggests that while storm events do not significantly alter the flux of POC and PON to depth, they may change POC and PON composition, given the change in source material and the hypothesis that diatoms, with their rapid sinking speeds, may transport fresher organic material to depth (Buesseler et al., 2007b).

4. Conclusions and Significance

The significance of this study is two-tiered in that it enabled: 1) the investigation of non-steady state and physical process ^{234}Th models, and 2) the impact of two storms on particle export. Most studies using ^{234}Th:^{238}U disequilibria use one-dimension SS models to derive particle export rates. In this study, the Lagrangian sampling strategy provided an ideal and rare opportunity to sample the same water mass multiple times over a given period (e.g. Savoye et al., 2006). This enabled the formulation of several ^{234}Th flux models that incorporated both NSS and physical process terms. Using a one-dimension NSS model, significant trends in integrated ^{234}Th activities resulted in unrealistic negative fluxes, suggesting that physical processes needed to be considered as well. The addition of a vertical upwelling term explained the observed ^{234}Th activities and enabled the determination of realistic upwelling rates of 2.2 to 3.7 m d^{-1}. While the assumptions used in the simple NSS, vertical upwelling box model are subject to large errors (accurate sediment trap fluxes, minimal patchiness), these results emphasize the importance of understanding the processes that control water column ^{234}Th derived particle export in low export regimes.

Given that both ^{234}Th derived particle export and sediment traps have inherent strengths and weaknesses, we used both to obtain a range in particle export estimates that result from the weather systems encountered during the cruise. Two transects were sampled, with the West Transect having relatively continuous convective mixing and the East Transect experiencing a pulsed convective mixing event. Export fluxes at 200 m ranged from 1.91 ± 0.20 to 4.92 ± 1.22 mmol C m^{-2} d^{-1}, 0.25 ± 0.08 to 0.54 ± 0.09 mmol N m^{-2} d^{-1}, and 0.22 ± 0.04 to 0.50 ± 0.06 mmol Si m^{-2} d^{-1} with generally higher fluxes associated with the eastern sampling. POC export efficiencies were not significantly different from the annual average or from winter time ambient conditions time periods without storms, although absolute POC fluxes were elevated by 1 - 11% over the

Sargasso Sea annual average of 869 ± 120 mmol C m^{-2} y^{-1} (Steinberg et al., 2001). This increase was not sufficient, however, to resolve the discrepancy between our observations and geochemical based estimates of particle export derived from net oxygen consumption, 2480 - 4160 mmol C m^{-2} y^{-1} (Jenkins, 1988; Jenkins and Goldman, 1985; Michaels et al., 1994). Comparison of PON export rates with simultaneous measurements of NO_3^- uptake derived new production rates, suggested that only a fraction, < 35%, of new production was exported as particles to deep waters during these events. Only a quarter of the remaining NO_3^- drawdown appears to accumulate as suspended PON or dissolved organic nitrogen (Lomas et al., 2008a), but the time scales of the various measurements and the natural variability associated with sub-mesoscale patchiness should not be ignored. Measured $bSiO_2$ export rates were more than a factor of two higher ($p < 0.01$) than the annual average for the Sargasso Sea, 0.07 – 0.14 mmol Si m^{-2} d^{-1} (Nelson and Brzezinski, 1997), with storm events contributing as much as 50%. Furthermore, a simple back of the envelope calculation suggests that 65 - 95% (average 86 ± 14%) of the total POC export measured was due to diatoms.

Combined these results suggest that while winter storms may increase primary and new production, they do not significantly increase POC and PON export to depth. Therefore, other mechanisms must be at work to resolve the ongoing discrepancy between direct POC flux measurements and geochemical observations. Thomalla et al. (2006) suggested that most POC export occurs in the temperate fringes of the North and South Atlantic Gyres and in regions characterized by continuous upwelling. Our results support that hypothesis. However, we do argue that storms play a substantial role in the export of $bSiO_2$ to deep waters, similar to that observed for other types of episodic events, such as mesoscale eddies in the Sargasso Sea and the sub-tropical Pacific Ocean (Benitez-Nelson et al., 2007; Buesseler et al., 2008; Maiti et al., 2008). Given the slower remineralization rates of $bSiO_2$ relative to POC and PON, we further hypothesize that this transport may, over time, slowly decrease water column silicate inventories, and further drive the Sargasso Sea towards increasing silica limitation. The implication that diatoms contribute disproportionately to the POC export observed during these storm events may impact the composition of the POC and PON being exported (e.g. Armstrong et al., 2002; Buesseler et al., 2007b) and therefore, the biological activity that occurs within the

mesopelagic zone. Thus, the role of winter storms in ocean biogeochemistry still needs to be investigated further.

Acknowledgements

We would like to thank the captain and crew of the R/V *Oceanus* and the entire science party, especially Mathieu Mongin, for their assistance in sample collection. CHN analyses were performed with the help of Eric Tappa and the $bSiO_2$ analyses by Renee Styles. We would also like to thank D.J. McGillicuddy (WHOI) for the sea level anomaly maps. The manuscript was significantly improved by three anonymous reviewers and Dr. Tom Trull. This study was funded by the National Science Foundation (Chemical Oceanography Grants OCE-0244612 and OCE-0241645).

References

Allen, J.T., Brown, L., Sanders, R., Moore, C.M., Mustard, A., Fielding, S., Lucas, M., Rixen, M., Savidge, G., Henson, S., Mayor, D., 2005. Diatom carbon export enhanced by silicate upwelling in the northeast Atlantic. Nature 437 (7059), 728-732.

Ammerman, J.W., Hood, R.R., Case, D.A., Cotner, J.B., 2003. Phosphorus deficiency in the Atlantic: an emerging paradigm in oceanography. EOS (Transactions, American Geophysical Union) 84, 165-170.

Armstrong, R., Lee, C., Hedges, J., Honjo, S., Wakeham, S., 2002. A new, mechanistic model for organic carbon fluxes in the ocean based on the quantitative association of POC with ballast minerals. Deep-Sea Research Part I-Oceanographic Research Papers 49, 219-236.

Baskaran, M., Santschi, P.H., Guo, L., Bianchi, T.S., Lambert, C., 1996. 234Th:238U disequilibria in the Gulf of Mexico: the importance of organic matter and particle concentration. Continental Shelf Research 16 (3), 353-380.

Benitez-Nelson, C.R., Bidigare, R.R., Dickey, T.D., Landry, M.R., Leonard, C.L., Brown, S.L., Nencioli, F., Rii, Y.M., Maiti, K., Becker, J.W., Bibby, T.S., Black, W., Cai, W.J., Carlson, C.A., Chen, F.Z., Kuwahara, V.S., Mahaffey, C., McAndrew, P.M., Quay, P.D., Rappe, M.S., Selph, K.E., Simmons, M.P., Yang, E.J., 2007. Mesoscale eddies drive increased silica export in the subtropical Pacific Ocean. Science 316 (5827), 1017-1021.

Benitez-Nelson, C.R., Buesseler, K.O., Karl, D.M., Andrews, J., 2001a. A time-series study of particulate matter export in the North Pacific Subtropical Gyre based on Th-234 : U-238 disequilibrium. Deep-Sea Research Part I-Oceanographic Research Papers 48 (12), 2595-2611.

Benitez-Nelson, C.R., Buesseler, K.O., van der Loeff, M.R., Andrews, J., Ball, L., Crossin, G., Charette, M.A., 2001b. Testing a new small-volume technique for determining Th-234 in seawater. Journal of Radioanalytical and Nuclear Chemistry 248 (3), 795-799.

Benitez-Nelson, C.R., Charette, M., 2004. Uncertainty versus variability in upper ocean carbon flux estimates. Limnology and Oceanography 49 (4), 1218-1220.

Bidigare, R.R., Benitez-Nelson, C.R., Leonard, C.L., Quay, P., Parsons, M.L., Foley, D.G., Seki, M.P., 2003. Influence of a cyclonic eddy on microheterotroph biomass and carbon export in the lee of Hawaii. Geophysical Research Letters 30 (6), 1318.

Brzezinski, M., 1985. The Si:C:N ratio of marine diatoms: interspecific variability and the effect of some environmental variables. Journal of Phycology 21 (347–357).

Brzezinski, M.A., 1992. Cell-cycle effects on the kinetics of silicic-acid uptake and resource competition among diatoms. Journal of Plankton Research 14 (11), 1511-1539.

Brzezinski, M.A., Kosman, C.A., 1996. Silica production in the Sargasso Sea during spring 1989. Marine Ecology-Progress Series 142 (1-3), 39-45.

Brzezinski, M.A., Nelson, D.M., 1995. The annual silica cycle in the Sargasso Sea near Bermuda Deep-Sea Research Part I-Oceanographic Research Papers 42 (7), 1215-1237.

Brzezinski, M.A., Nelson, D.M., Franck, V.M., Sigmon, D.E., 2001. Silicon dynamics within an intense open-ocean diatom bloom in the Pacific sector of the Southern Ocean. Deep Sea Research Part II: Topical Studies in Oceanography 48 (19-20), 3997-4018.

Brzezinski, M.A., Phillips, D.R., 1997. Evaluation of ^{32}Si as a tracer for measuring silica production rates in marine waters. Limnology and Oceanography 42 (5), 856-865.

Buesseler, K., Ball, L., Andrews, J., Benitez-Nelson, C.R., Belastock, R., Chai, F., Chao, Y., 1998. Upper ocean export of particulate organic carbon in the Arabian Sea derived from thorium-234. Deep-Sea Research Part Ii-Topical Studies in Oceanography 45 (10-11), 2461-2487.

Buesseler, K.O., Andrews, J.A., Hartman, M.C., Belastock, R., Chai, F., 1995. Regional estimates of the export flux of particulate organic carbon derived from Th-234 during the JGOFS EqPAC program. Deep-Sea Research Part Ii-Topical Studies in Oceanography 42 (2-3), 777-804.

Buesseler, K.O., Andrews, J.E., Pike, S.M., Charette, M.A., Goldson, L.E., Brzezinski, M.A., Lance, V.P., 2005. Particle export during the southern ocean iron experiment (SOFeX). Limnology and Oceanography 50 (1), 311-327.

Buesseler, K.O., Antia, A.N., Chen, M., Fowler, S.W., Gardner, W.D., Gustafsson, O., Harada, K., Michaels, A.F., Rutgers van der Loeff, M., Sarin, M., Steinberg, D.K., Trull, T., 2007a. An assessment of the use of sediment traps for estimating upper ocean particle fluxes. Journal of Marine Research 65, 345-416.

Buesseler, K.O., Bacon, M.P., Cochran, J.K., Livingston, H.D., 1992. Carbon and Nitrogen Export During the JGOFS North-Atlantic Bloom Experiment Estimated from Th-234:U-238 Disequilibria. Deep-Sea Research Part a-Oceanographic Research Papers 39 (7-8A), 1115-1137.

Buesseler, K.O., Benitez-Nelson, C.R., Moran, S.B., Burd, A., Charette, M., Cochran, J.K., Coppola, L., Fisher, N.S., Fowler, S.W., Gardner, W., Guo, L.D., Gustafsson, O., Lamborg, C., Masque, P., Miquel, J.C., Passow, U., Santschi, P.H., Savoye, N., Stewart, G., Trull, T., 2006. An assessment of particulate organic carbon to thorium-234 ratios in the ocean and their impact on the application of Th-234 as a POC flux proxy. Marine Chemistry 100 (3-4), 213-233.

Buesseler, K.O., Benitez-Nelson, C.R., Rutgers van der Loeff, M., Andrews, J., Ball, L., Crossin, G., Charette, M.A., 2001. An intercomparison of small- and large-volume techniques for thorium-234 in seawater. Marine Chemistry 74 (1), 15-28.

Buesseler, K.O., Lamborg, C., Cai, P., Escoube, R., Johnson, R., Pike, S., Masque, P., McGillicuddy, D.J., Verdeny, E., 2008. Particle fluxes associated with mesoscale eddies in the Sargasso Sea. Deep Sea Research II, 55(14-15), 1522-1539.

Buesseler, K.O., Lamborg, C.H., Boyd, P.W., Lam, P.J., Trull, T.W., Bidigare, R.R., Bishop, J.K.B., Casciotti, K.L., Dehairs, F., Elskens, M., Honda, M., Karl, D.M., Siegel, D.A., Silver, M.W., Steinberg, D.K., Valdes, J., Van Mooy, B., Wilson, S., 2007b. Revisiting carbon flux through the ocean's twilight zone. Science 316 (5824), 567-570.

Buesseler, K.O., Michaels, A.F., Siegel, D.A., Knap, A.H., 1994. A 3-dimensional time-dependent approach to calibrating sediment trap fluxes. Global Biogeochemical Cycles 8 (2), 179-193.

Burd, A.B., Moran, S.B., Jackson, G.A., 2000. A coupled adsorption-aggregation model of the POC/234Th ratio of marine particles. Deep Sea Research Part I: Oceanographic Research Papers 47 (1), 103-120.

Chen, J.H., edwards, R. L., Wasserburg, B.J., 1986. 238U, 234U and 232Th in seawater. Earth and Planetary Science Letters 80, 241-251.

Cochran, J.K., Hirschberg, D.J., Livingston, H.D., Buesseler, K.O., Key, R.M., 1995. Natural and anthropogenic radionuclide distributions in the Nansen Basin, Arctic Ocean: Scavenging rates and circulation timescales. Deep-Sea Research Part Ii-Topical Studies in Oceanography 42 (6), 1495-1517.

Cochran, J.K., Roberts, K.A., Barnes, C., Achman, D., 1997. Radionuclides as indicators of particle and carbon dynamics on East Greenland Shelf. Radioprotection - Colloques 32 (C2), 129-136.

Cullen, J.J., Franks, P.J.S., Karl, D.M., Longhurst, A., 2002. Physical influences on marine ecosystem dynamics. In: Robinson, A.R., McCarthy, J.J., Rothschild, B.J. (Eds.), The Sea: Biological-Physical Interactions in the Ocean. John Wiley and Sons, pp. 297-335.

Dickey, T., Zedler, S., Yu, X., Doney, S.C., Frye, D., Jannasch, H., Manov, D., Sigurdson, D., McNeil, J.D., Dobeck, L., Gilboy, T., Bravo, C., Siegel, D.A., Nelson, N., 2001. Physical and biogeochemical variability from hours to years at the Bermuda Testbed Mooring site: June 1994-March 1998. Deep-Sea Research Part Ii-Topical Studies in Oceanography 48 (8-9), 2105-2140.

Ditullio, G.R., Laws, E.A., 1991. Impact of an atmospheric oceanic disturbance on phytoplankton community dynamics in the North Pacific Central Gyre. Deep-Sea Research Part a-Oceanographic Research Papers 38 (10), 1305-1329.

Dugdale, R.C., Wilkerson, F.P., 1998. Silicate regeneration of new production in the equatorial Pacific upwelling. Nature 391, 270-273.

Dunne, J., Murray, J., 1999. Sensitivity of 234Th export to physical processes in the central equatorial Pacific. Deep Sea Research I 46, 831-854.

Eppley, R.W., Peterson, B.J., 1979. Particulate organic matter flux and planktonic new production in the deep ocean. Nature 282, 677-680.

Faure, G., Mensing, T.M., 2005. Isotopes: Principles and Applications. John Wiley and Sons.

Gardner, W.D., Chung, S.P., Richardson, M.J., Walsh, I.D., 1995. The Oceanic Mixed-Layer Pump. Deep-Sea Research II 42 (2-3), 757-765.

Jenkins, W.J., 1988. Nitrate flux into the euphotic zone near Bermuda. Nature 331 (6156), 521-523.

Jenkins, W.J., Doney, S.C., 2003. The subtropical nutrient spiral. Global Biogeochemical Cycles 17 (4).

Jenkins, W.J., Goldman, J.C., 1985. Seasonal oxygen cycling and primary production in the Sargasso Sea. Journal of Marine Research 43 (2), 465-491.

Karl, D.M., Dore, J.E., Lukas, R., Michaels, A.F., Bates, N.R., Knap, A.H., 2001. Building the long-term picture: The U.S. JGOFS time-series programs. Oceanography 14 (4), 6-17.

Knap, A.H., Michaels, A.F., Steinberg, D., Bahr, F., Bates, N., Bell, S., Countway, P., Close, A., Doyle, A., Howse, F., Gundersen, K., Johnson, R., Little, R., Orcutt, K., Parsons, R., Rathbun, C., Sanderson, M., Stone, S., 1997. U.S. Joint Global Ocean Flux Study, Bermuda Atlantic Time-series Study. BATS methods manual. U.S. JGOFS Planning and Coordination Office, Woods Hole, MA.

Knauer, G.A., Martin, J.H., Bruland, K.W., 1979. Fluxes of particulate carbon, nitrogen, and phosphorus in the upper water column of the northeast Pacific. Deep Sea Research Part A. Oceanographic Research Papers 26, 97-108.

Krause, J.W., Nelson, D.M., Lomas, M.W., 2008. Biogenic silica production and export in the Sargasso Sea during late winter storms prior to seasonal stratification. Deep-Sea Research I, submitted.

Lamborg, C.H., Buesseler, K.O., Valdes, J., Bertrand, C.H., Bidigare, R., Manganini, S., Pike, S., Steinberg, D., Trull, T., Wilson, S., 2008. The flux of bio- and lithogenic material associated with sinking particles in the mesopelagic "twilight zone" of the northwest and North Central Pacific Ocean. Deep Sea Research Part II: Topical Studies in Oceanography 55 (14-15), 1540-1563.

Lipschultz, F., 2001. A time-series assessment of the nitrogen cycle at BATS. Deep-Sea Research II 48, 1897-1924.

Lipschultz, F., Bates, N.R., Carlson, C.A., Hansell, D.A., 2002. New production in the Sargasso Sea: History and current status. Global Biogeochemical Cycles 16 (1), art. no.-1001, doi:10.1029/2000GB001319.

Lomas, M.W., Lipschultz, F., DM, N., Krause, J.W., Bates, N.R., 2008a. Biogeochemical responses to late-winter storms in the Sargasso Sea. I. Pulses of primary and new production. Deep Sea Research I, in press.

Lomas, M.W., Roberts, N., Lipschultz, F., Krause, J.W., Nelson, D.M., Bates, N.R., 2008b. Biogeochemical responses to late-winter storms in the Sargasso Sea. III. Rapid succession of major phytoplankton grounps. Deep Sea Research I, submitted.

Maiti, K., 2007. Effects of transient processes on particle dynamics in marine systems. Ph.D., University of South Carolina, Columbia.

Maiti, K., Benitez-Nelson, C.R., Rii, Y., Bidigare, R.R., 2008. The influence of a mature cyclonic eddy on particle export in the lee of Hawaii. Deep Sea Research II 55, 1445-1460.

Martin-Jezequel, V., Hildebrand, M., Brzezinski, M.A., 2000. Silicon metabolism in diatoms: Implications for growth. Journal of Phycology 36 (5), 821-840.

McGillicuddy, D.J., Anderson, L.A., Bates, N.R., Bibby, T., Buesseler, K.O., Carlson, C.A., Davis, C.S., Ewart, C., Falkowski, P.G., Goldthwait, S.A., Hansell, D.A., Jenkins, W.J., Johnson, R., Kosnyrev, V.K., Ledwell, J.R., Li, Q.P., Siegel, D.A., Steinberg, D.K., 2007. Eddy/wind interactions stimulate extraordinary mid-ocean plankton blooms. Science 316 (5827), 1021-1026.

Michaels, A.F., Knap, A.H., Dow, R.L., Gundersen, K., Johnson, R.J., Sorensen, J., Close, A., Knauer, G.A., Lohrenz, S.E., Asper, V.A., Tuel, M., Bidigare, R., 1994. Seasonal patterns of ocean biogeochemistry at the United-States JGOFS Bermuda Atlantic Time-Series Study Site. Deep-Sea Research Part I-Oceanographic Research Papers 41 (7), 1013-1038.

Michaels, A.F., Silver, M.W., 1988. Primary Production, Sinking Fluxes and the Microbial Food Web. Deep-Sea Research Part a-Oceanographic Research Papers 35 (4), 473-490.

Nelson, D., Brzezinski, M., 1997. Diatom growth and productivity in an oligotrophic midocean gyre: A 3-yr record from the Sargasso Sea near Bermuda. Limnology and Oceanography 42 (3), 473-486.

Paasche, E., 1973. Silicon and the ecology of marine plankton diatoms. I. *Thalassiosira pseudonana (Cyclotella nana)* grown in a chemostat with silicate as limiting nutrient. Marine Biology 19, 117-126.

Painter, S.C., Sanders, R., Poulton, A.J., Malcolm, E., Woodward, S., Lucas, M., Chamberlain, K., 2007. Nitrate uptake at photic zone depths is not important for export in the subtropical ocean. Global Biogeochemical Cycles 21, GB4005, doi:10.1029/2006GB002807.

Pesant, S., Legendre, L., Gosselin, M., Bauerfeind, E., Budeus, G., 2002. Wind-triggered events of phytoplankton downward flux in the Northeast Water Polynya. Journal of Marine Systems 31 (4), 261-278.

Pike, S., Buesseler, K., Andrews, J., Savoye, N., 2005. Quantification of 234Th recovery in small volume sea water samples by inductively coupled plasma mass spectrometry. Journal of Radioanalytical and Nuclear Chemistry 263 (2), 355-360.

Ragueneau, O., Tréguer, P., Leynaert, A., Anderson, R.F., Brzezinski, M.A., DeMaster, D.J., Dugdale, R.C., Dymond, J., Fischer, G., François, R., Heinze, C., Maier-Reimer, E., Martin-Jézéquel, V., Nelson, D.M., Quéguiner, B., 2000. A review of the Si cycle in the modern ocean: recent progress and missing gaps in the application of biogenic opal as a paleoproductivity proxy. Global and Planetary Change 26 (4), 317-365.

Rutgers van der Loeff, M., Sarin, M.M., Baskaran, M., Benitez-Nelson, C., Buesseler, K.O., Charette, M., Dai, M., Gustafsson, Ö., Masque, P., Morris, P.J., Orlandini, K., Rodriguez y Baena, A., Savoye, N., Schmidt, S., Turnewitsch, R., Vöge, I., Waples, J.T., 2006. A review of present techniques and methodological advances in analyzing 234Th in aquatic systems. Marine Chemistry 100 (3-4), 190-212.

Savoye, N., Benitez-Nelson, C., Burd, A.B., Cochran, J.K., Charette, M., Buesseler, K.O., Jackson, G.A., Roy-Barman, M., Schmidt, S., Elskens, M., 2006. Th-234 sorption and export models in the water column: A review. Marine Chemistry 100 (3-4), 234-249.

Smayda, T.J., 1998. Patterns of variability characterizing marine phytoplankton, with examples from Narragansett Bay. ICES Journal of Marine Science 55 (4), 562-573.

Steinberg, D.K., Carlson, C.A., Bates, N.R., Johnson, R.J., Michaels, A.F., Knap, A.H., 2001. Overview of the US JGOFS Bermuda Atlantic Time-series Study (BATS): a decade-scale look at ocean biology and biogeochemistry. Deep-Sea Research Part Ii-Topical Studies in Oceanography 48 (8-9), 1405-1447.

Strickland, J.D.H., Parsons, T.R., 1972. A Practical Handbook of Seawater Analysis. Fisheries Research Board of Canada, Ottawa.

Thomalla, S., Turnewitsch, R., Lucas, M., Poulton, A., 2006. Particulate organic carbon export from the North and South Atlantic gyres: The 234Th/238U disequilibrium approach. Deep Sea Research Part II: Topical Studies in Oceanography 53 (14-16), 1629-1648.

Tsunogai, S., Noriki, S., Harada, K., Kurosaki, T., Watanabe, Y., Maedaa, M., 1986. Large but variable particulate flux in the Antarctic Ocean and its significance for the chemistry of Antarctic water Journal of Oceanographic Society of Japan 42 (2), 83-90.

Walker, N.D., Leben, R.R., Balasubramanian, S., 2005. Hurricane-forced upwelling and chlorophyll a enhancement within cold-core cyclones in the Gulf of Mexico. Geophysical Research Letters 32 (18).

Wei, C.L., Murray, J.W., 1992. Temporal variations of 234Th activity in the water column of Dabob Bay: Particle Scavenging. Limnology and Oceanography 37, 297-314.

Figure Legends:

Figure 1: Map of study area showing the sampling location along the West and East Transects. The location of the BATS station is identified by a gray star.

Figure 2: Net heat flux and estimated mixed layer depth (MLD) for the West (A, B) and East (C, D) transects.

Figure 3: Depth versus density (kg m^{-3}) profiles along West (A) and East (B) transects.

Figure 4: Temporal variability in $^{234}Th/^{238}U$ ratios and along the West (A) and East (B) Transect.

Figure 5: Calculated ^{234}Th export at 200 m using both steady state (dark gray) and non-steady state (light gray) models and assuming negligible physical processes for each station along the West and East Transects.

Figure 6: Time-series of the depth weighted total ^{234}Th activities over progressively deeper layers for the West Transect. Solid line is the best fit to a linear decrease in total ^{234}Th versus time and the dashed line represent 95% confidence limit around this slope (see Table 2).

Figure 7: Time series of the depth weighted total ^{234}Th activities over progressively deeper layers for the East Transect. Solid line is the best fit to a linear decrease in total ^{234}Th versus time and the dashed line represent 95% confidence limit around this slope (see Table 2).

Figure 8: Model for showing the temporal evolution of 0 – 200 m depth weighted total ^{234}Th activity for West (A) and East (B) transects. The solid diamond line represents ^{238}U activity, solid circle represents observed ^{234}Th activity, hollow squares represent expected ^{234}Th activity with ingrowth and decay, hollow diamonds represents ^{234}Th activity with

ingrowth, decay and export and hollow triangle represents ^{234}Th activity with ingrowth, decay, export and external input.

Figure 9: Estimated particle fluxes at 200 m using sediment traps and ^{234}Th derived measurements. The dotted lines represent average winter particle flux estimates of 1552 ± 1091 μmol C m^{-2} d^{-1}, 221 ± 172 μmol N m^{-2} d^{-1} (1990-2002; BATS data) and 108 ± 50 μmol $bSiO_2$ m^{-2} d^{-1} respectively (1992-1994; Nelson and Brzezinski, 1997) .

List of Tables:

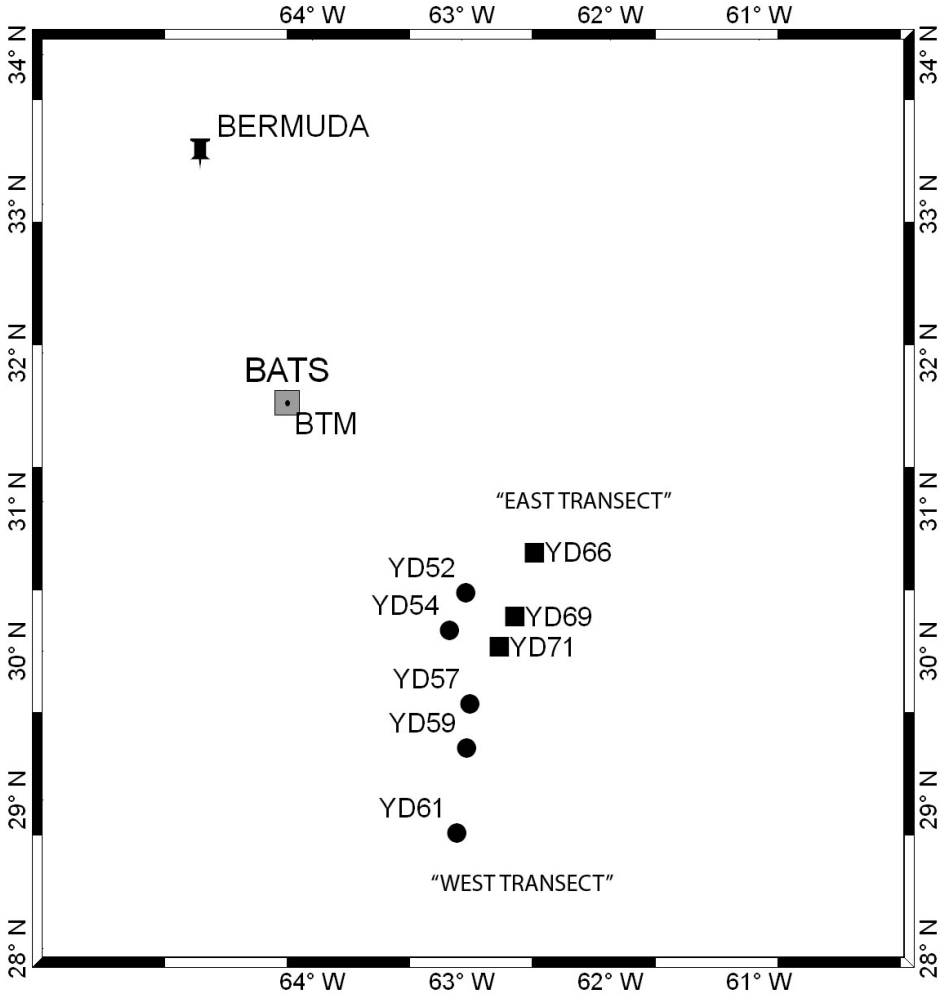

Maiti et al. Figure 1.

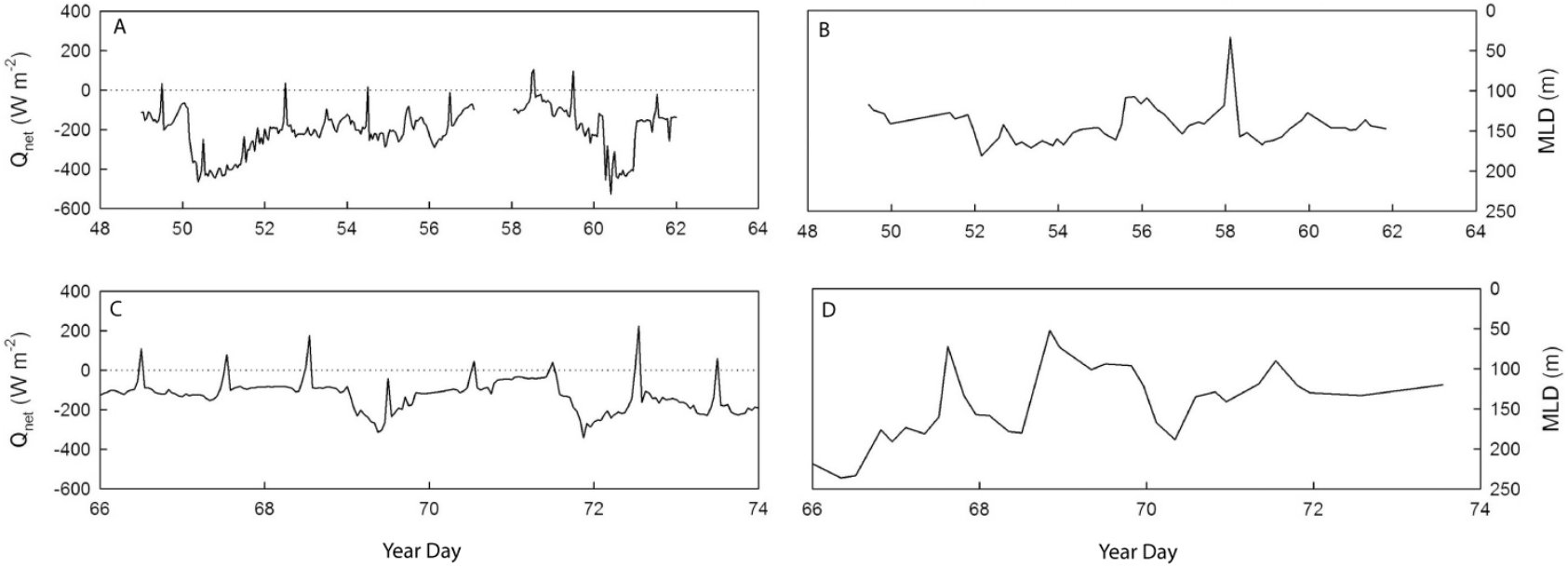

Maiti et al. Figure 2.

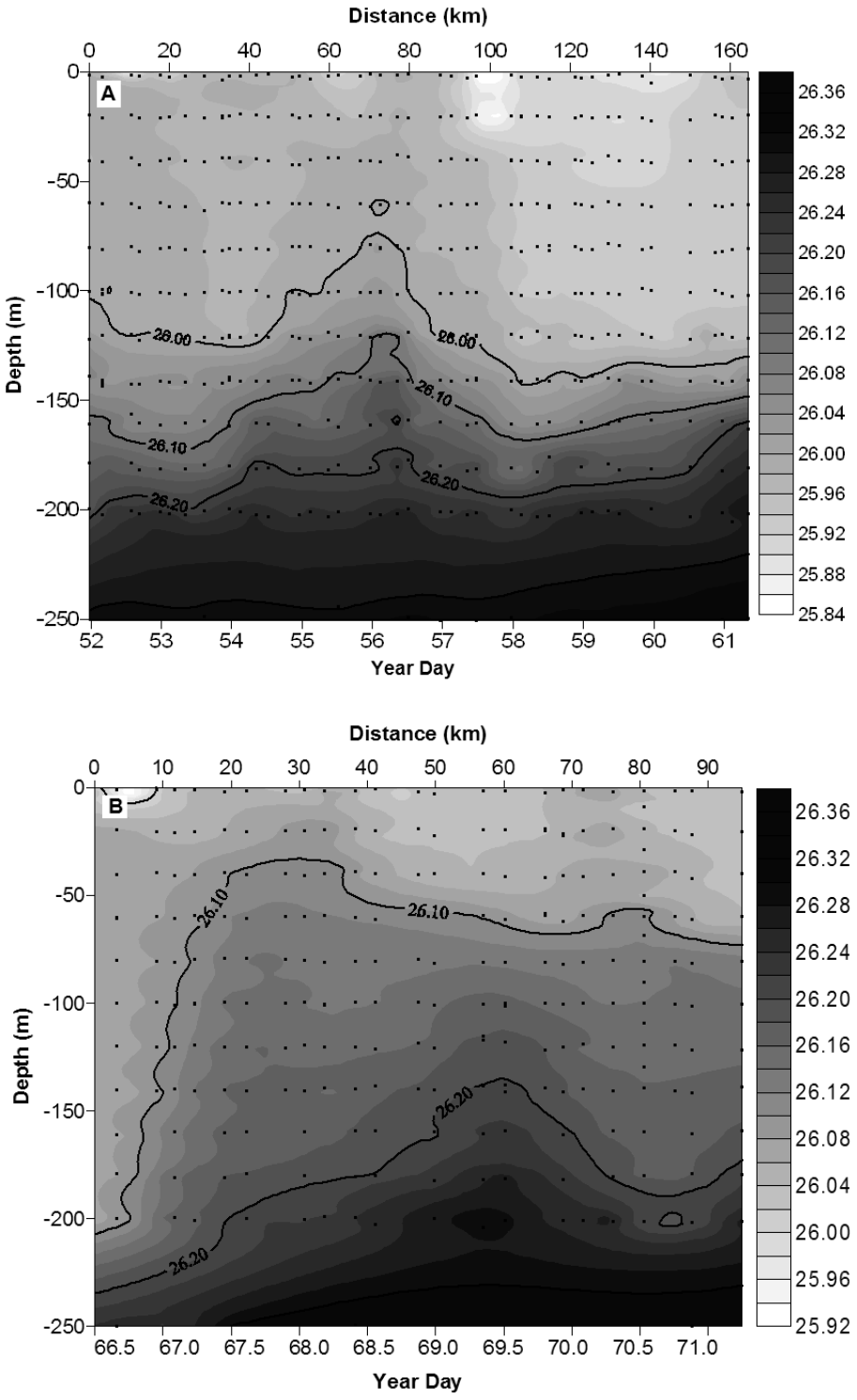

Maiti et al Figure 3.

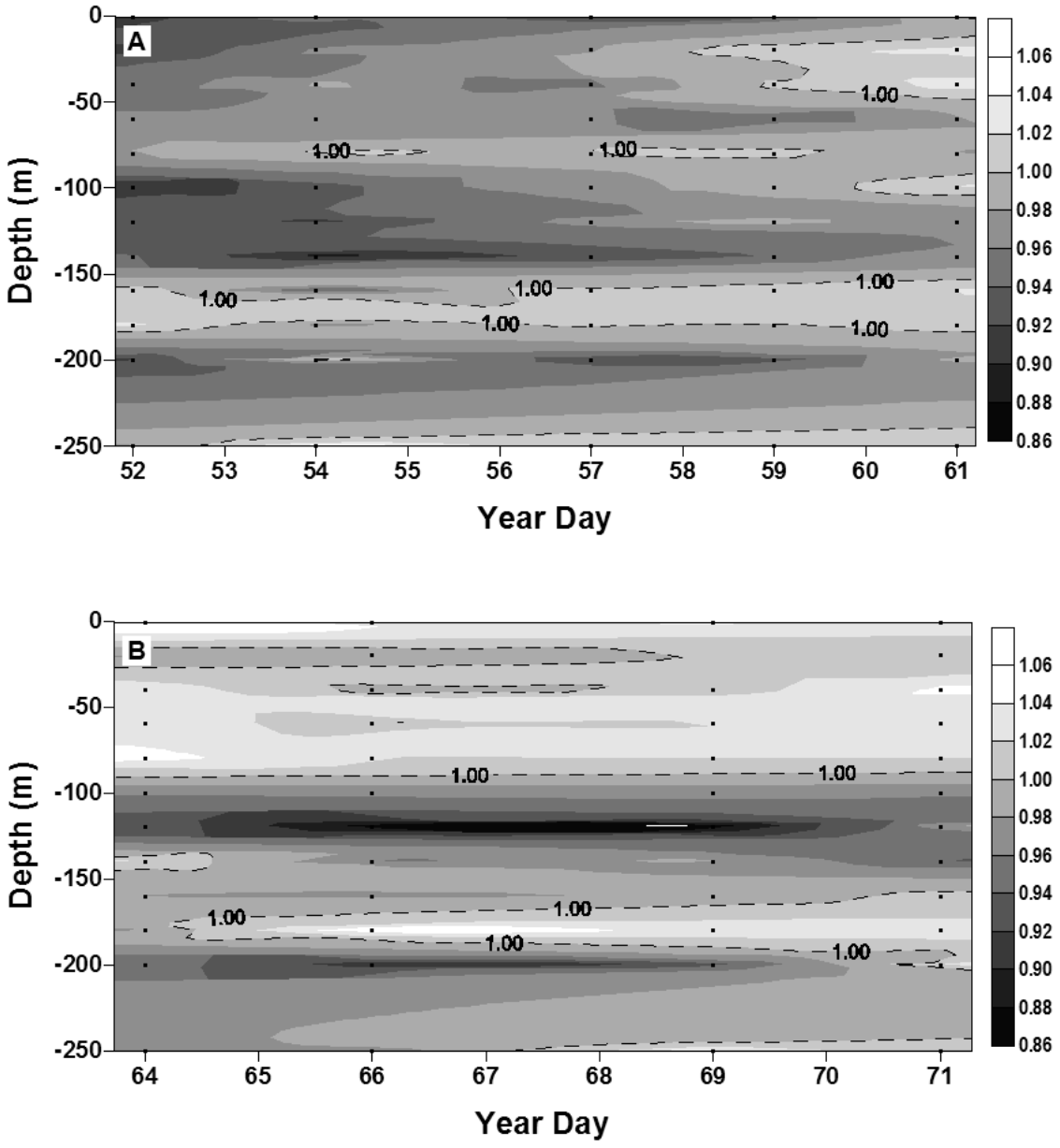

Maiti et al Figure 4.

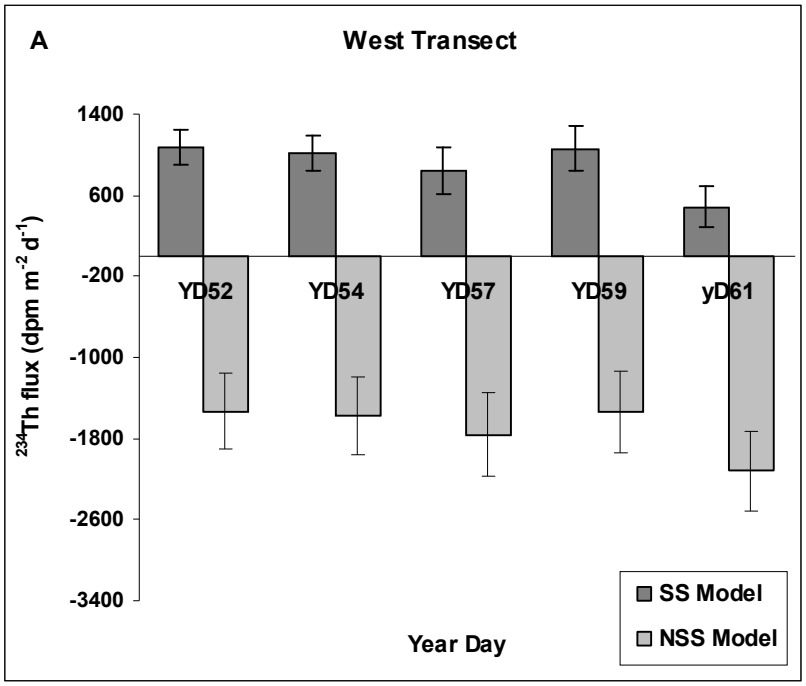

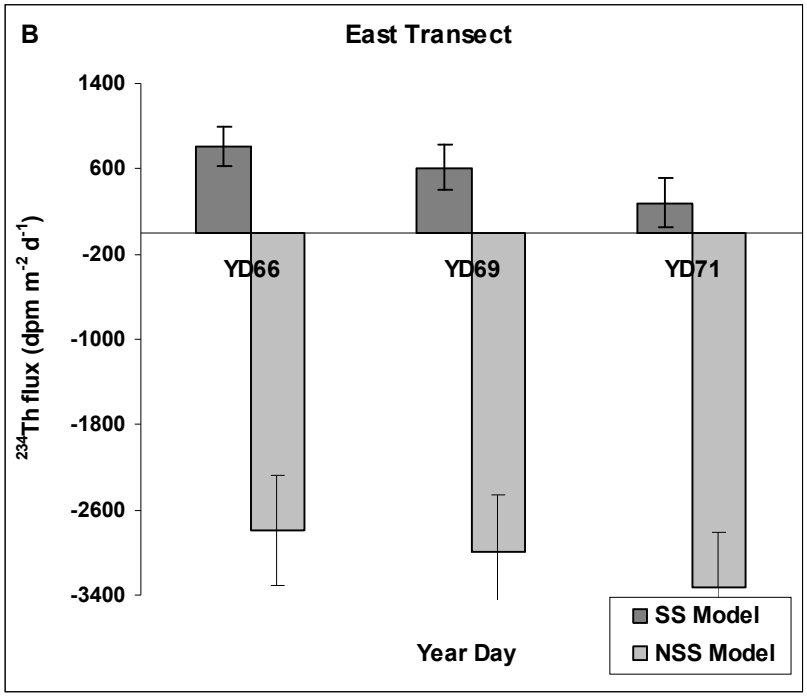

Maiti et al. Figure 5

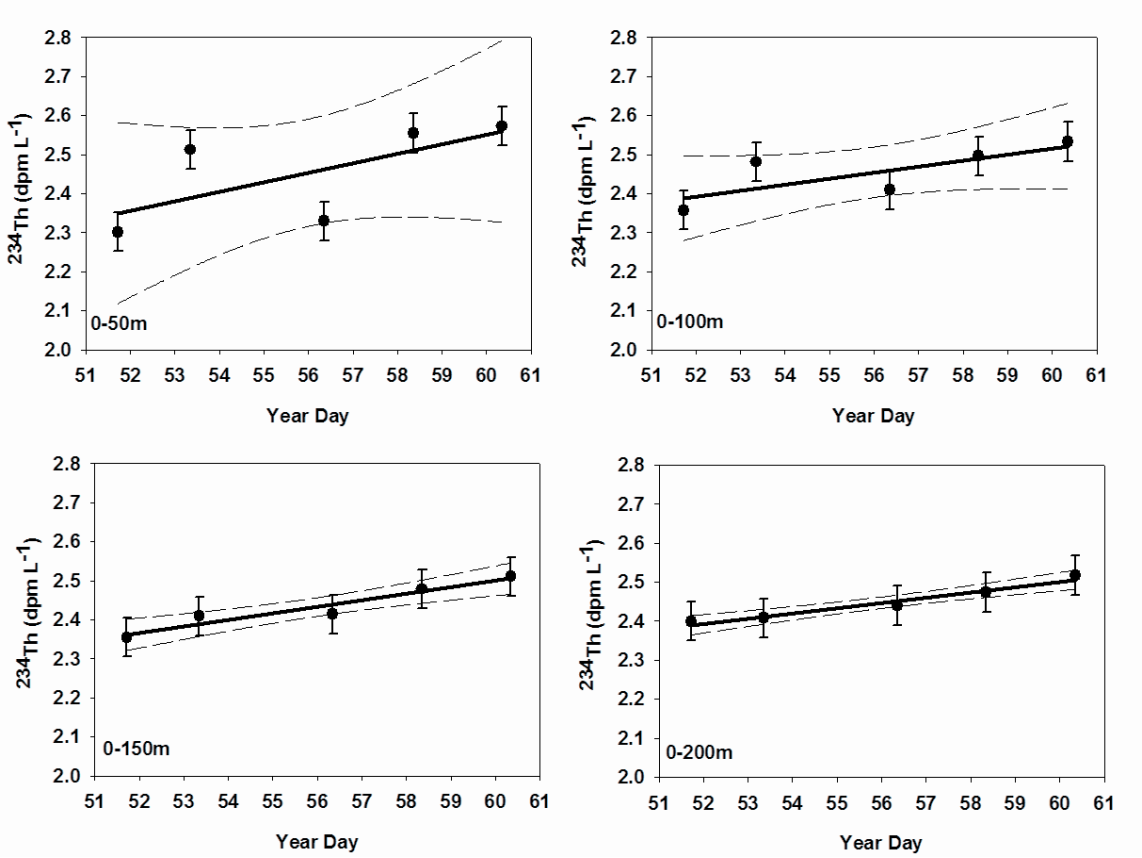

Maiti et al. Figure 6.

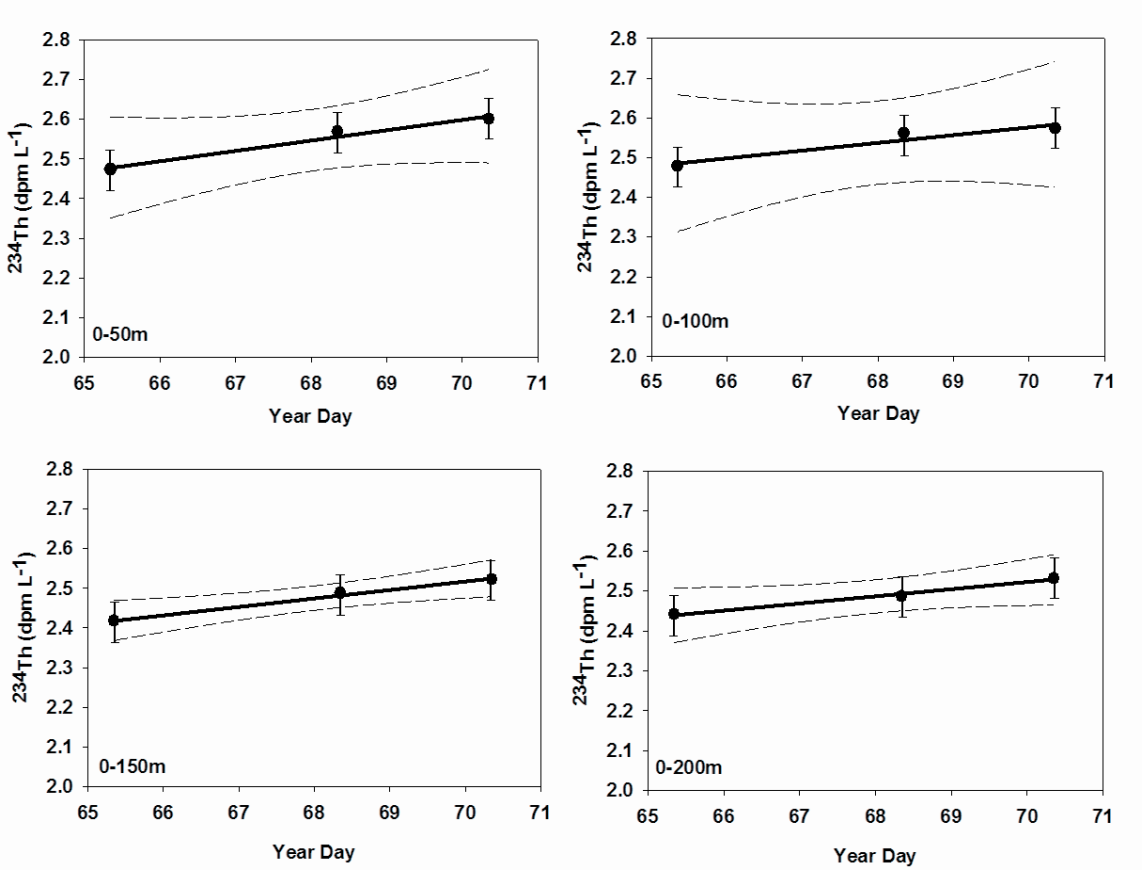

Maiti et al. Figure 7.

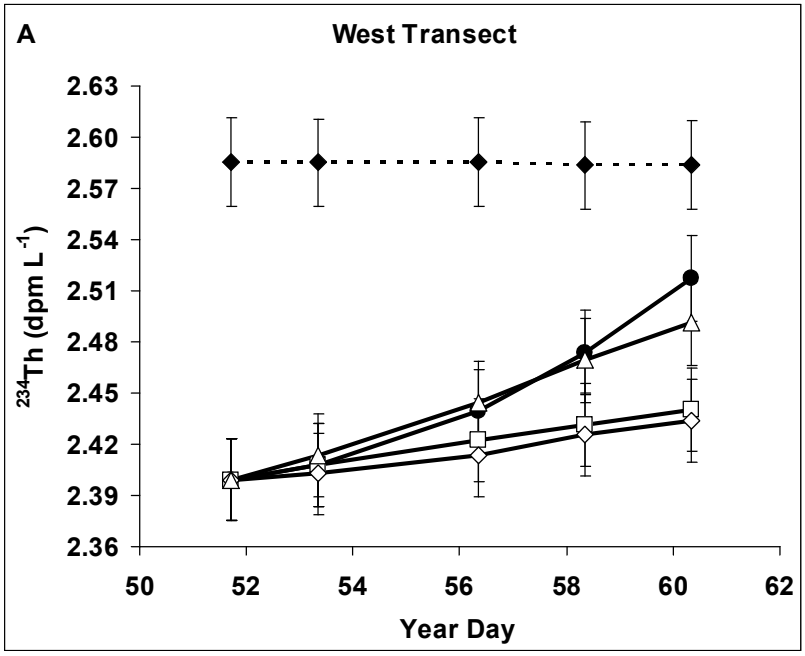

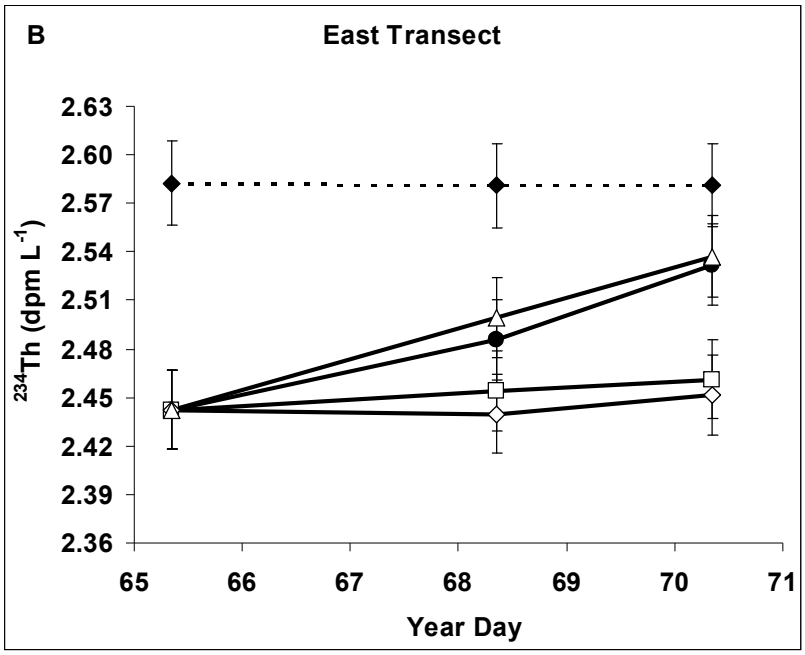

Maiti et al. Figure 8.

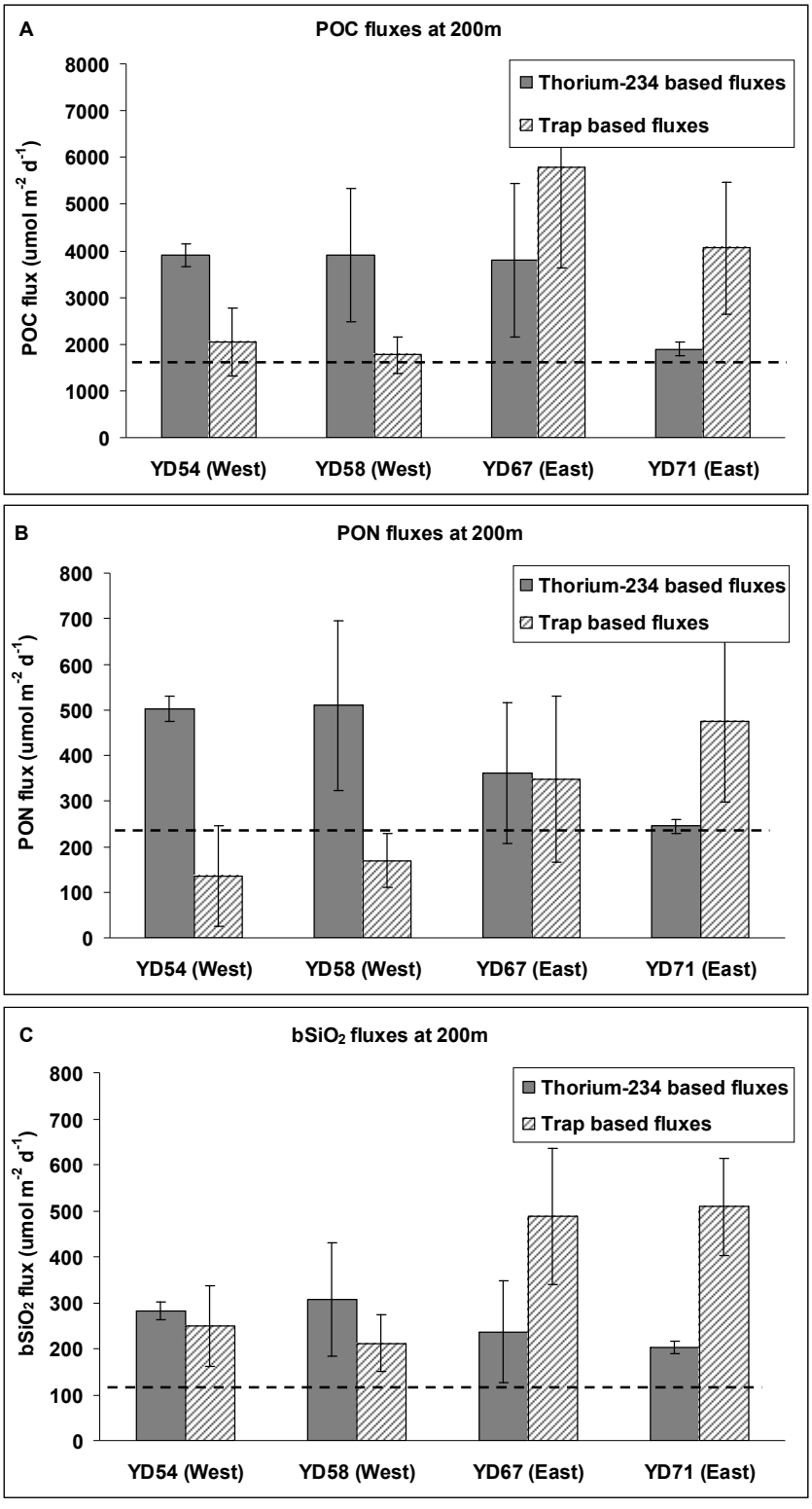

Maiti et al. Figure 9.

Table 1: ^{234}Th fluxes at 200m estimated using SS and NSS models and assuming negligible physical processes.

Station	Transect	^{234}Th flux (SS model)	^{234}Th flux (NSS model)	^{234}Th flux (sediment trap)
		dpm m^{-2} d^{-1}	dpm m^{-2} d^{-1}	dpm m^{-2} d^{-1}
YD52	West	1071 ± 175	-1529 ± 380	772 ± 76
YD54	West	1020 ± 174	-1580 ± 380	
YD57	West	840 ± 232	-1760 ± 410	462 ± 55
YD59	West	1064 ± 224	-1536 ± 405	
YD61	West	484 ± 197	-2116 ± 391	
YD66	East	808 ± 205	-2792 ± 511	1150 ± 124
YD69	East	615 ± 232	-2985 ± 522	
YD71	East	283 ± 197	-3318 ± 508	763 ± 91

Table 2: Time dependent regression of ^{234}Th activity over different depth ranges for the West and East transects.

	Transect	0-50m	0-100m	0-150m	0-200m
Slope ($\partial Th/\partial t$) (dpm L^{-1} d^{-1}	West	0.024	0.015	0.017	0.013
% error in slope	West	65%	48%	16%	13%
R^2	West	0.44	0.59	0.93	0.95
Slope ($\partial Th/\partial t$)	East	0.026	0.019	0.021	0.018
% error in slope	East	17%	31%	8%	13%
R^2	East	0.97	0.91	0.99	0.98

Table 3. Integrated abundance (10^{11} cells m^{-2}) of *Prochlorococcus* (~0.6um diameter), *Synechococcus* (~1um diameter), Picoeukaryotes (~1-3um diameter) and Nanoeukaryotes (~3-10um diameter) as determined by flow cytometry (Lomas et al., 2008b).

	Prochlorococcus	Synechococcus	Picoeukaryotes	Nanoeukaryotes
West Transect 0-100m	32.2 ± 8.8	13.6 ± 2.1	0.84 ± 0.16	0.08 ± 0.024
0-160m	39.8 ± 10.4	17.98 ± 2.5	1.33 ± 0.4	0.1 ± 0.03
East Transect 0-100m	9.1 ± 4.3	20.7±7.9	3.13 ± 1.5	0.33 ± 0.16
0-160m	12.1 ± 7.4	28.1 ± 16.5	4.46 ± 2.74	0.47 ± 0.19

Note: Data are the average (± stdev) of all values collected for the same latitudinal range (30 – 30.5°N) so that the averages are not biased by the increase in smaller cells as one approaches the inter-tropical convergence zone. For all averages there are five separate profiles of cell abundance.

Table 4: Estimate of particle fluxes at 200 m.

Elemental flux at 200m	Transect	^{234}Th based fluxes	Trap based fluxes	Average of ^{234}Th and trap based estimates (± std. dev.)	Average of both methods and both transects (± std. dev.)
		mmol m^{-2} d^{-1}	mmol m^{-2} d^{-1}	mmol m^{-2} d^{-1}	mmol m^{-2} d^{-1}
POC	West	3.90 ± 0.32	1.91 ± 0.20	2.90 ± 1.16	3.39 ± 1.39
	East	2.85 ± 1.34	4.92 ± 1.22	3.89 ± 1.59	
PON	West	0.50 ± 0.17	0.25 ± 0.08	0.33 ± 0.20	0.34 ± 0.14
	East	0.30 ± 0.08	0.54 ± 0.09	0.36 ± 0.09	
$bSiO_2$	West	0.29 ± 0.05	0.23 ± 0.03	0.26 ± 0.04	0.31 ± 0.05
	East	0.22 ± 0.04	0.50 ± 0.06	0.36 ± 0.16	